Exosomes promote axon outgrowth and a polarized neuronal morphology by engaging the Wnt-Planar Cell Polarity pathway

Samar Ahmad[1], Melanie Pye[2], Masahiro Narimatsu[2], Siyuan Song[1], Tania Christova[1], Jeffrey L. Wrana[2], Liliana Attisano[1]

[1]Department of Biochemistry, Donnelly Centre, University of Toronto, Toronto, ON, M5S 3E1, Canada

[2]Center for Systems Biology, Lunenfeld-Tanenbaum Research Institute, Mt. Sinai Hospital and Department of Molecular Genetics, University of Toronto, Toronto, Ontario M5G 1X5, Canada

Corresponding author: liliana.attisano@utoronto.ca

Abstract

In neurons, the acquisition of a polarized morphology is achieved upon the outgrowth of a single axon from one of several neurites. Exosomes from diverse sources are known to promote the neurite outgrowth, however, the role of fibroblast-derived exosomes on axon elongation in neurons of the central nervous system under growth permissive conditions remains unclear. Here, we show that fibroblast-derived exosomes promote axon outgrowth and a polarized neuronal morphology in mouse primary embryonic cortical neurons. Mechanistically, we demonstrate that the exosome-induced increase in axon outgrowth requires endogenous Wnts and core PCP components including Prickle, Vangl, Frizzled and Dishevelled. We demonstrate that exosomes are internalized by neurons, colocalize with Wnt7b and induce relocalization of Vangl2 to the distal axon during axon outgrowth. In contrast, exosomes derived from neurons or astrocytes do not promote axon outgrowth, while exosomes from activated astrocytes inhibit elongation. Thus, our data reveals that fibroblast-derived exosomes promote axon elongation through the Wnt-PCP pathway in a manner that is dependent on endogenous Wnts.

Introduction

Neurons are the fundamental unit of the central nervous system (CNS) and exhibit a polarized morphology comprised of a single long axon and one or multiple dendrites. Sensory signals are received by dendrites and propagated down the length of the axon to neighboring neurons (Arimura & Kaibuchi, 2007; Namba *et al*, 2015; Schelski & Bradke, 2017; Takano *et al*, 2019). Thus, proper neuronal morphology is critical for synaptic transmission and cognitive functions of the brain. To acquire a polarized morphology, one neurite outgrows the other minor neurites and forms an axon, a process referred as neuronal polarization (Arimura & Kaibuchi, 2007; Namba *et al.*, 2015; Schelski & Bradke, 2017; Takano *et al.*, 2019). Axons differ in their growth potential such that during development axons grow rapidly but in the adult CNS, axons have lost the ability to grow (Bradke, 2022). Hence, the study of the mechanisms of axon growth during development can provide insights into processes that need to be reactivated during axon regeneration in adults. Diverse extracellular factors have been reported to modulate neurite outgrowth and neuronal polarization (Arimura & Kaibuchi, 2007; Namba *et al.*, 2015; Schelski & Bradke, 2017; Takano *et al.*, 2019). Extracellular vesicles (EVs), including exosomes, are membranous structures that arise from multivesicular bodies (MVBs) within the endosomal pathway. Exosomes range in size from 30-150 nm and harbour a variety of biomolecules including proteins, DNA and RNAs (Colombo *et al*, 2014; Pegtel & Gould, 2019; van Niel *et al*, 2022). Exosomes regulate many processes including immune responses, wound healing and disease pathology (Zhang *et al*, 2019; Yates *et al*, 2022; Buzas, 2023). In the CNS, exosomes act as carriers for communication among neurons and glia, and promote neuroprotective functions (Chivet *et al*, 2013; Bahram Sangani *et al*, 2021; Gassama & Favereaux, 2021; Fan *et al*, 2022). The biological activities of exosomes depend upon the features of the cells from which they originate. For instance, exosomes from mesenchymal stem cells increase the number of neurites and promote neurite outgrowth in cortical neurons (Xin *et al*, 2012; Lopez-Verrilli *et al*, 2016; Zhang *et al*, 2017) while those from Schwann cells of the peripheral nervous system (PNS) promote axon regeneration in PNS neurons (Lopez-Verrilli *et al*, 2013). Peripheral nerve fibroblast-derived exosomes promote Schwann cell-mediated myelination of neurons (Zhao *et al*, 2022). Moreover, fibroblasts promote sorting of Schwann cells at an injury site that leads to axon regrowth (Parrinello *et al*, 2010). Thus, both fibroblasts and Schwann cells contribute to the remarkable regenerative ability of the PNS. In the context of growth inhibitory substrates, it has been shown that exosomes from fibroblasts can

promote axon regeneration in cortical neurons (Tassew *et al*, 2017). However, the direct effect of fibroblast-derived exosomes on axon outgrowth of CNS neurons during growth permissive conditions remain unclear.

Exosomes have previously been shown to mobilize autocrine Wnt-Planar cell polarity (PCP) signaling in breast cancer cells (Luga *et al*, 2012). PCP signaling was first described for its function in modulating tissue polarity by aligning cells in a single plane, perpendicular to the apical-basal axis (Goodrich & Strutt, 2011; Yang & Mlodzik, 2015; Devenport, 2016; Koca *et al*, 2022). In vertebrates, PCP signaling also functions in the development of inner ear, orientation of hair follicles and convergent extension (CE) movements during gastrulation and neural tube closure (Jones & Chen, 2007; Wallingford, 2012; Butler & Wallingford, 2017; Davey & Moens, 2017; Wang *et al*, 2019; Montcouquiol & Kelley, 2020). In the CNS, PCP modulates numerous developmental processes including differentiation of neural progenitor cells, neuronal migration, axon guidance and dendritic arborization (Goodrich, 2008; Davey & Moens, 2017; Hakanen *et al*, 2019; Zou, 2020). Core components of the PCP pathway are the seven-pass transmembrane Frizzled (Fzd) receptors, four-pass transmembrane Van-Gogh-like (Vangl) proteins, and cytoplasmic proteins including Prickle (Pk) and Dishevelled (Dvl) (Goodrich & Strutt, 2011; Yang & Mlodzik, 2015; Devenport, 2016; Koca *et al.*, 2022). Unlike in Drosophila, Wnt morphogens play an important role in regulating PCP signaling in vertebrates, and may act as an instructive cue (Butler & Wallingford, 2017).

Wnts are lipid-modified secreted glycoproteins that act as morphogens to regulate processes during embryonic development including cell proliferation and fate, polarity and migration (Willert & Nusse, 2012; Nusse & Clevers, 2017; Steinhart & Angers, 2018; Mittermeier & Virshup, 2022; Rim *et al*, 2022). In neurons, Wnts are known to modulate dendritogenesis, axon guidance and remodelling, synaptogenesis, synaptic plasticity and differentiation (Salinas, 2012; Bonansco *et al*, 2022). In mammals, there are 19 Wnts that bind to different classes of cell surface receptors and trigger diverse cellular responses (Rim *et al.*, 2022). Wnt receptors and co-receptors include members of Fzd, low-density lipoprotein related receptor (LRP) and receptor tyrosine kinases (RTKs) such as ROR, RYK, and PTK7 (MacDonald & He, 2012; Niehrs, 2012). Despite

increasing knowledge about Wnt signaling, little is known about the role of Wnt-PCP pathway in axon outgrowth.

The current study was aimed at investigating the contribution of Wnt-PCP signaling in exosome-induced axon outgrowth. We show that exosomes derived from diverse fibroblast cell lines promote axon outgrowth that leads to acquisition of a polarized neuronal morphology. Mechanistically, we show that the exosome-induced increase in axon outgrowth requires neuronally-expressed Wnts and PCP components including Pk, Vangl, Fzd and Dvl. Importantly, we show that exosomes are internalized by neurons where they can colocalize with Wnt7b and also induce a shift in Vangl2 localization towards distal part of axon. In contrast to fibroblast-derived exosomes, those isolated from neurons or astrocytes do not alter axon outgrowth, while exosomes isolated from activated astrocytes inhibit axon outgrowth.

Results

Exosomes promote acquisition of a polarized neuronal morphology by enhancing axon outgrowth

Dissociated primary mouse embryonic cortical neurons when freshly plated *in vitro* (Fig. S1A) give rise to short neurites, one of which grows rapidly to form an axon by 24-48 hours to generate a polarized neuron (Dotti *et al*, 1988; Arimura & Kaibuchi, 2007). Recent studies have demonstrated that exosomes isolated from mesenchymal stem cells can promote neurite outgrowth (Lopez-Verrilli *et al.*, 2016; Zhang *et al.*, 2017). Thus, we sought to explore the role of fibroblast-derived exosomes in neurite outgrowth. We first isolated and characterized exosomes from diverse mouse and human fibroblast cell culture supernatants including mouse L cells, mouse embryonic fibroblasts (MEFs), human dermal fibroblasts (HDFn), normal human lung fibroblasts (NHLF) and BJ foreskin fibroblasts using differential centrifugation (Fig. 1A). Analysis of the final pellet by immunoblotting revealed the presence of exosome markers CD81, TSG101 and Flotillin1, and the absence of the endoplasmic reticulum (ER)-resident protein, Calnexin (CNX) (Fig. 1B). Particle size distribution analysis of the final pellet using nanoparticle tracking analysis (NTA) showed that the majority of particles were within a size range of 30-150 nm (Fig. 1C) that is characteristic of exosomes (Colombo *et al.*, 2014). Ultrastructural analysis by transmission

electron microscopy (TEM) further showed intact round vesicles ranging in sizes of 30-150 nm in diameter, thus, confirming the identity and structural integrity of the isolated exosomes (Fig. 1D).

We next investigated the role of the fibroblast purified exosomes on the neuronal morphology using dissociated E15.5 – 16.5 primary mouse embryonic cortical neurons. Neurons were treated 4 h after plating with exosomes for either 20 or 29 hours and were fixed and stained with Tuj1 antibody, which detects the neuron specific β-III tubulin. Quantification of neurite lengths revealed that exosomes from all five fibroblast lines enhanced the length of the longest neurite (ie the prospective axon) from a mean of ~30 μm (in controls) to ~60 μm at 24 h and from ~40 μm (in controls) to ~75 μm at 33 hours (Fig. 1E and F). In contrast, the individual lengths (~10 μm) and the total combined length (~20 μm) of the remaining neurites, excluding the longest, referred to as minor neurites and correspond to prospective dendrites, remained unchanged (Fig. 1G and H). The total number of neurites was also unaltered by exosome treatment (Fig. 1I). Similarly, when neurons were treated with varying concentrations of exosomes (0.05-10 μg/mL) obtained from all five fibroblast cell lines, a dose-dependent increase in the length of the longest neurite at both 24 and 33 hours was observed with the maximal effect occurring at 5 μg/mL (Fig. S1B-K). To verify that exosomes preferentially act on axons, neurons treated with exosomes from L cells were co-stained with the axonal marker, Tau-1 and the dendritic marker, MAP2. Quantification of Tau-1 positive axons confirmed that exosomes increased the length of axons (Fig. S2A and B), yielding results similar to those obtained when the length of the longest neurite, independent of Tau-1 staining was quantified in parallel (Fig. S2C). Similar to the data observed in Fig. 1G, the length of individual neurites (~10 μm) positive for the dendritic marker MAP2 was unaffected by exosomes (Fig. S2D). Moreover, exosome treatment concordantly resulted in a significant increase in the percent of neurons with Tau-positive axons, a characteristic of a polarized neuron that was clearly evident within 24 h of plating (Fig. S2E). Taken together, these results demonstrate that exosomes derived from a variety of fibroblast lines, promote axon outgrowth and accordingly enhance the acquisition of a polarized phenotype.

Next, to confirm our observations and to rule out a potential role for contaminating cell membranes or protein aggregates in mediating the effects on neuronal morphology, we undertook two different and more stringent exosome isolation protocols, where the final ultracentrifugation (100,000 x g)

pellet of exosomes obtained from L cell supernatants was further subjected to either density gradient purification (Fig. S3) or size exclusion chromatography (Fig. S4). For density gradient separation, the resuspended pellet was applied to a discontinuous iodixanol gradient and then subjected to an additional ultracentrifugation (Fig. S3A). Characterization of the floating fractions by immunoblotting demonstrated that Fractions 6 – 8 were positive for the exosome markers, CD81 and Flotillin1 (Fig. S3B) with the intensity of both markers peaking in Fraction 7 (Fig. S3C). Of note, Fraction 9 had the highest amount of total protein but very low levels of exosome markers (Fig. S3C) indicating a successful enrichment of exosomes particles in Fractions 6 - 8. Particle size distribution analysis showed that the number of particles peaked at approximately 100 nm, which is a characteristic of exosomes, and that the Fraction 7 had the highest number of particles (Fig. S3D). Moreover, Fraction 7 (F7) had the highest particle/protein ratio (Fig. S3E), a parameter that is widely used to measure the purity of EVs (Webber & Clayton, 2013; Thery *et al*, 2018). Treatment of dissociated neurons with these purified exosomes from the F7 fraction revealed that the length of the longest neurite (ie the prospective axon) was increased to levels similar to that observed for the initial ultracentrifugation pellet (Exo) at all time points (Fig. S3F and S3G).

Next, we used size exclusion chromatography as an alternative approach to purify exosomes from the ultracentrifugation (100,000 x g) pellets (Fig. S4A). Characterization of the isolated fractions revealed the presence of the exosomal markers, CD81, Flotillin1 and Tsg101 but not the ER protein, Calnexin (CNX) in fractions 7 – 12 (Fig. S4B), with particle size peaking at a diameter of approximately 100 nm with fraction F7 having the highest particle/protein ratio (Fig. S4C and D) which is characteristic of exosomes. Treatment of dissociated neurons with F7 purified exosomes revealed that the length of the longest neurite (ie the prospective axon) was increased to levels similar to that observed for the initial ultracentrifugation pellet (Exo) at both 24 and 33 hours (Fig. S4E and F) as observed previously (Fig. 1E, 1F and S1). Of note, outgrowth induced by exosomes isolated using either purification method was easily detected as early as 12 hours (ie 8 h after exosome addition), highlighting that the rapid nature of the response (Fig. S3F and G and Fig. S4E and F).

Altogether, these observations suggest that the exosomes isolated by ultracentrifugation (100,000 x g pellet) are responsible for promoting axon outgrowth. Since the responses induced by these

pelleted exosomes were similar to that achieved after more extensive purifications, we used this ultracentrifuged pellet as a source of exosomes for all subsequent experiments.

The PCP pathway is required for exosome-induced growth of the prospective axon

Previous work has demonstrated that in cancer cells, motility induced by exogenously added fibroblast-derived exosomes is mediated by the Wnt planar cell polarity pathway (PCP) in recipient cells (Luga *et al.*, 2012). Prickle (Pk) and Vangl, core PCP components, distribute asymmetrically to the proximal side in planar polarized epithelial cells (Yang & Mlodzik, 2015; Butler & Wallingford, 2017) and are also known to modulate neuronal morphology (Dreyer *et al*, 2022; Radaszkiewicz *et al*, 2023). This prompted us to investigate whether core PCP components might be required for exosome-induced axon outgrowth. To study this, we used a combination of siRNA-mediated knockdown and mouse genetic models to explore the role of these core PCP components in dissociated primary cortical neurons. There are two Prickle genes, Prickle 1 and Prickle 2 (Pk1 and Pk2), expressed in cortical neurons (Fig. S5A). To test for the requirement for Prickle, neurons were co-transfected with siRNAs targeting Pk1 and/or Pk2 along with plasmid, encoding GFP to visualize transfected cells. Analysis of GFP positive neurons in which expression of Pk1 and Pk2 alone or together was abrogated, revealed that neurons were comprised solely of minor neurites (mean length ~10 μM), none of which were elongated upon treatment with exosomes (Fig. 2A and 2B). Knockdown efficiency was confirmed by qPCR after FACS sorting for GFP positive neurons (Fig. 2C). As an alternative to this transient approach, we explored the consequences on neuronal morphology using dissociated neurons isolated from mice with genetic loss of Pk1 or Pk2. While Pk2 knockout mice are viable (Tao *et al*, 2011), Pk1 knockout mice display early embryonic lethality (Tao *et al*, 2009). Thus, we generated mice with single floxed Pk alleles ($Pk1^{f/f}$ and $Pk2^{f/f}$) using targeted homologous recombination (Fig. S5B), which were then crossed with each other to obtain mice with double ($Pk1^{f/f}$;$Pk2^{f/f}$) floxed Pk alleles. Both single and double floxed mice, after removal of neomycin cassette, were viable, fertile, and exhibited no overt anatomical defects. Conditional knockout mice were then generated by crossing with Nestin-Cre mice to achieve loss of Pk1/2 in the developing brain. Loss of Pk1/2 expression in the cortex of $Pk1^{f/f}$;$Pk2^{f/f}$;Nestin-Cre E15.5 embryos was confirmed by immunofluorescence microscopy using Pk1 and Pk2 antibodies (Fig. S5C and S5D). Consistent with the siRNA results, analysis of cortical neurons (E15.5-16.5) isolated from mice with a Nestin-Cre conditional deletion of either Pk1 alone, Pk2 alone or both

(Pk1$^{f/f}$;Pk2$^{+/+}$;Nestin-Cre, Pk1$^{+/+}$;Pk2$^{f/f}$;Nestin-Cre or Pk1$^{f/f}$;Pk2$^{f/f}$;Nestin-Cre, respectively) revealed the presence of only short neurites that failed to elongate in response to exosome treatment in contrast to the Pk1$^{+/+}$;Pk2$^{f/f}$ or Pk1$^{+/+}$; Pk2$^{+/+}$;Nestin-Cre controls (Fig. 2D and S5E). We next explored the contribution of the core PCP tetraspanin proteins, Vangl1 and Vangl2, which regulate diverse aspects of neuronal development (Dreyer *et al.*, 2022). Vangl2 is expressed at much higher levels than Vangl1 (ie ~30x) in cortical neurons (Fig. S5A) and consistent with this, abrogation of Vangl2 expression using siRNAs preferentially decreased exosome-mediated induction of outgrowth of the longest neurite with only modest effects observed for Vangl1 (Fig. 2E-G). Loop-tail mice harbor a S464N point mutation in the Vangl2 allele (Kibar *et al*, 2001; Murdoch *et al*, 2001) that results in reduced Vangl2 protein levels and defective translocation to plasma membrane (Torban *et al*, 2007; Merte *et al*, 2010; Belotti *et al*, 2012). Morphological examination showed that the heterozygous loop-tail embryos (Vangl2$^{+/Lp}$) exhibited a curly tail with partial or no neural tube defects, whereas homozygous loop-tail embryos (Vangl2$^{Lp/Lp}$) exhibited a completely open neural tube (Fig. 2H) as previously reported (Kibar *et al.*, 2001). Consistent with the siRNA results, dissociated cortical neurons isolated from E15.5 – 16.5 Vangl2$^{Lp/Lp}$ embryos, but not wild-type or heterozygotes (Lp/+) displayed short neurites (~ 10 μM in length) and a loss of exosome-induced outgrowth of the longest neurite at both 24 and 33 hours (Fig. 2I and S5F).

Smurf1 and Smurf2 are E3 ubiquitin ligases that modulate PCP signaling to control convergent extension, cell protrusion and motility (Wang *et al*, 2003; Sahai *et al*, 2007; Narimatsu *et al*, 2009; Luga *et al.*, 2012) and have also been shown to play a key role in regulating neuronal morphology (Vohra *et al*, 2007; Cheng *et al*, 2011; Kannan *et al*, 2012). Since cortical neurons express both Smurf1 and Smurf2 as determined by RNA sequencing analysis (Fig. S5A), we next explored whether Smurfs might have a role in exosome-induced axon outgrowth. For this, we examined the contribution of Smurf1 and/or Smurf2 using dissociated neurons isolated from Smurf knockout mice. Smurf1$^{+/-}$;Smurf2$^{+/-}$ double heterozygotes (Narimatsu *et al.*, 2009) were crossbred to generate offspring with varying Smurf1/2 genotypes. Analysis of dissociated cortical neurons revealed that complete loss of either Smurf1 alone (Smurf1$^{-/-}$; Smurf2$^{+/+}$) or Smurf2 alone (Smurf1$^{+/+}$;Smurf2$^{-/-}$) yielded neurons that harboured only short neurites (~ 10 μM in length) and that exosome-induced outgrowth of the longest neurite was prevented in contrast to wild-type or

heterozygote (Smurf1$^{+/-}$;Smurf2$^{+/-}$) littermates (Fig. S5G and S5H). These results suggest that Smurf1 and Smurf2 act in a non-redundant manner or that a minimal level of combined Smurf1/2 activity is required for neurite outgrowth.

Both PCP and canonical β–catenin signaling is initiated upon binding of Wnt ligands to one of 10 members of the seven-pass transmembrane Frizzled family of receptors (Fzd) and is then propagated intracellularly through one of three Dishevelleds (Dvls) (van Amerongen *et al*, 2008; Gao & Chen, 2010; MacDonald & He, 2012; Yang & Mlodzik, 2015; Wang *et al*, 2016; Sharma *et al*, 2018). Thus, we next explored which Fzds and Dvls are required for exosome-mediated axon outgrowth. Cortical neurons treated with a pan-Fzd blocking antibody (F2.A) that recognizes multiple Fzds, including Fzd1, 2, 4, 5, 7 and 8 (Pavlovic *et al*, 2018; Tao *et al*, 2019) displayed only minor neurites that failed to elongate in response to exosomes (Fig. 3A and 3B). Mouse E15.5-16.5 cortical neurons express Fzd1, 2, 3, 7, 8 and 9 with Fzd1 and Fzd3 displaying the highest levels (Fig. S5A), thus we next explored the individual requirement for these receptors using siRNAs. Quantification revealed that individual loss of Fzd1, 3 or 9 yielded neurons with minor neurites that failed to elongate in response to exosomes while loss of Fzd7 only blocked exosome mediated outgrowth (Fig. 3C, S6A and B). Loss of Fzd2 or Fzd8 had no effect, though equivalent knockdown efficiency was achieved (Fig. S6B). These results indicate that multiple but specific Fzds (Fzd 1, 3 and 9) are required for axon specification and/or basal elongation, whereas only Fzd7 is specifically required for exosome-mediated outgrowth of the prospective axon. All three Dishevelleds (Dvl1, 2 and 3) are expressed in cortical neurons with Dvl1 being expressed at the highest level (Fig. S5A). Analysis of the requirement for Dvls using siRNAs revealed that only Dvl2 was required for exosome-induced outgrowth (Fig. 3D, S6C and D).

Individual Fzds and Dvls function in both PCP and β-catenin pathways in a complex and highly redundant manner thus it is challenging to associate specific Fzds/Dvls to a particular pathway (Gao & Chen, 2010; Mlodzik, 2016; Wang *et al.*, 2016). However it is worth noting that evidence of Fzd7 and Dvl2, both of which we observed to be specifically required for exosome-induced growth of the prospective axon, have been reported to function in PCP pathways (Zou, 2020; Pascual-Vargas & Salinas, 2021). Taken together, these observations suggest that core PCP

components are required for the axon specification and/or elongation and that they are required for exosome-induced growth of the longest neurite.

Vangl2 localizes asymmetrically during exosome-induced growth of the longest neurite

Prior work has revealed that Wnt5a mediated activation of the PCP pathway in dissociated commissural neurons results in relocalization of Vangl2 to the growth cone (Shafer *et al*, 2011). Thus, we next explored whether exosomes might similarly promote relocalization of Vangl2. In control (PBS) or exosome-treated embryonic cortical neurons, Vangl2 was distributed in both the somal membrane and in the axon but in distinct patterns (Fig. 3E). Quantification of Vangl2 distribution within the axon shaft revealed that in controls, a preferential localization in the proximal half of the axon was observed (Fig. 3F). Remarkably, in neurons treated with exosomes for 20 h, Vangl2 relocalized to the distal end of the axon (50% versus 10% in controls) and was often detected within the growth cone (Fig. 3F). No overt change in Vangl2 localization in the somal membrane was observed. This re-localization of Vangl2 to the distal axon and growth cone suggests that exosomes engage PCP components to promote axon growth.

Autocrine Wnts mediate exosome induced growth of the longest neurite

Wnts, including Wnt5a, Wnt7a and Wnt7b can promote axon elongation, neurogenesis and axon guidance, respectively, via the PCP pathway (Salinas, 2012; Bonansco *et al.*, 2022). As exosomes are known to carry Wnts (Routledge & Scholpp, 2019; Gross, 2021; Mittermeier & Virshup, 2022), we next explored whether the presence of Wnt ligands in isolated exosomes could contribute to the observed outgrowth of neurites. We first abrogated the expression of porcupine, an acyltransferase essential for Wnt lipidation and secretion (Mikels & Nusse, 2006; Takada *et al*, 2006) in the exosome-producing L cells using siRNAs and isolated the exosomes (Fig. 4A). Abrogation of Porcupine expression had no effect on the overall number of exosomes secreted or on the levels of the exosome markers, CD81, Flotillin1 and TSG101 as indicated by immunoblotting (Fig. S7A-D). Moreover, ultrastructural analysis by TEM revealed intact round, exosome-like vesicles in both the control and Porcupine knockdown samples (Fig. S7E). When applied to cortical neurons, exosomes isolated from Porcupine-deficient L cells were as active as control exosomes in promoting outgrowth of the longest neurite (Fig. 4B-D). These results thereby

indicate that the activity of L cell-derived exosomes was not due to the presence of Wnts within the exosomes.

We next sought to determine whether L cell-secreted exosomes might modulate autocrine Wnt signaling in neurons to promote neurite outgrowth. To investigate this, we blocked the ability of neurons to secrete Wnts by chemically inhibiting the activity of Porcupine using IWP2 or LGK974 (Chen *et al*, 2009; Liu *et al*, 2013) (Fig. 4E). This analysis revealed that treatment of cortical neurons with Porcupine inhibitors prevented exosome-mediated neurite outgrowth (Fig. 4F and G). The Wnt carrier protein, Wntless (Wls) is required for Wnt secretion (Banziger *et al*, 2006), and abrogating expression of Wls using siRNAs, similarly prevented exosome-induced axon outgrowth (Fig. 4H-J). Thus, blocking pathways essential for Wnt secretion prevents exosome-induced growth of the longest neurite, indicating that neuronally-expressed endogenous Wnts are necessary for exosome function.

Analysis of RNA sequencing results revealed that cortical neurons express Wnt5a, Wnt5b, Wnt7a and Wnt7b (Fig. S5A). We verified by qPCR that these Wnts were expressed and that expression levels remain constant throughout the time frame of the experiment (Fig. S7F). Thus, to determine which Wnts are important for neurite outgrowth, the expression of each Wnt was individually abrogated using siRNAs (Fig. S7G). Neurons lacking Wnt5b, Wnt7a or Wnt7b but not Wnt5a were comprised solely of minor neurites, none of which elongated upon treatment with exosomes (Fig. 4K and 4L). Altogether, these observations suggest that exogenously added exosomes might mobilize endogenous Wnts (Wnt5b, Wnt7a and Wnt7b) to promote growth of the longest neurite.

Exosomes associate with Wnts during neurite outgrowth

To explore exosome uptake in neurons, we used a compartmentalized microfluidic chamber device (Taylor *et al*, 2005) comprised of a set of proximal compartments, where neurons are seeded, and a set of distal compartments where axons emerge. The compartments are connected by a microgroove barrier that enables a gradient based fluidic separation due to the hydrostatic pressure (Fig. 5A). Plated neurons were grown for 5 days to allow axons to reach the distal compartment. Exosomes were added to either compartment for 24 hours and then neurons were fixed and stained

for Tuj1. Addition of exosomes to the proximal compartment containing the cell bodies but not to the distal compartment containing axon tips, promoted elongation of neurites (Fig. 5B and 5C).

To directly visualize exosome uptake, we used conditioned media (CM) from L cells stably expressing CD81-EYFP as a source of EYFP-labelled exosomes (Luga *et al.*, 2012). Immunoblotting of both the conditioned media (CM) and the exosome pellet revealed the presence of EYFP using an anti-GFP antibody (Fig. 5D and 5E), indicating successful integration of the CD81-EYFP fusion protein in exosomes. Neurons were treated with the CM from either control or CD81-EYFP expressing L cells for 29 hours. Immunostaining followed by confocal microscopy revealed that the majority of GFP-positive neurons displayed abundant GFP puncta within the soma as well as occasional staining in the axon, suggesting that exosomes were internalized (Fig. 5F). Next, neurons were incubated with CM containing CD81-EYFP-labelled exosomes for 30 minutes, washed and subsequently chased in regular CM media for varying times prior to fixation. We found that exosomes were internalized by neurons within the 30 min exposure time, and that the internalized exosomes were found both in the soma and in axons throughout the time course (0 - 24 hours) (Fig. 5G). Thus, exosomes are rapidly (within 30 min) taken up by neurons and can be detected as long as 24 h later.

In cancer cells, internalized exosomes acquire endogenous Wnts to activate PCP signaling (Luga *et al.*, 2012). Given that exosomes were internalized in neurons, we next investigated whether the internalized exosomes could associate with the Wnts. Cortical neurons were electroporated with HA-tagged Wnt7b (Wnt7b-HA) or empty vector control and 24 hours after plating were treated with EYFP-labelled exosomes for 30 min. Immunostaining with anti-HA and GFP antibody showed colocalization of Wnt7b-HA and exosomes in the soma (Fig. S7H). Next, we examined whether exosomes were colocalized with endogenous Wnt7b, the ligand most highly expressed in neurons. Neurons were treated with 10X concentrated CM obtained from either control or CD81-EYFP expressing L cells for 30 min and then were fixed and immunostained with anti-GFP and anti-Wnt7b antibodies, whose specificity was first confirmed by immunofluorescence microscopy (Fig. S7I). This analysis revealed colocalization of Wnt7b and exosomes in both the soma and axon (Fig. 5H and I). Given that internalized exosomes colocalize with Wnt7b, and that

endogenous Wnts are required for exosome induced outgrowth, our findings suggest that internalized exosomes may acquire neuronally expressed Wnt7b to promote axon outgrowth.

Exosomes from neurons and astrocytes do not promote neurite outgrowth

In the brain, exosomes mediate glia-neuron communication during developmental processes and pathogenesis (Chivet *et al.*, 2013; Bahram Sangani *et al.*, 2021; Gassama & Favereaux, 2021; Fan *et al.*, 2022). Neurons and astrocytes are the two major cell types in the CNS, and are known to secrete exosomes (Gassama & Favereaux, 2021). Thus, we sought to determine whether exosomes released from neurons or astrocytes also modulate neurite outgrowth. To examine this, we first isolated and tested exosomes produced by primary embryonic cortical neurons (Fig. 6A). Exosome pellets were positive for exosomal markers and displayed the typical 30-150 nm diameter size range (Fig. S8A and B). However, in contrast to fibroblast-derived exosomes, these exosomes did not promote neurite outgrowth when added to neurons at any dose tested, including at concentrations much higher (0.05-10 μg/mL) than those required for fibroblast-derived exosome effects (Fig. 6B and C). Thus, exosomes exogenously secreted from neurons do not promote neurite outgrowth.

Astrocytes support many physiological functions of neurons including synapse development and neuronal activity, whereas reactive astrocytes produced during injury or aging (Clarke *et al*, 2018) contribute to the production of the inhibitory environment that prevents axon regeneration (Clarke & Barres, 2013; Pekny & Pekna, 2014; Liddelow & Barres, 2017; Lee *et al*, 2022). Thus, we next investigated the role of astrocyte-derived exosomes on neurite outgrowth (Fig. 6A). For this, we isolated primary mouse astrocytes from newborn pups at postnatal day (P) 1-4 and confirmed their identity by positive staining for GFAP (Fig. S8C) and negative staining for the neuronal marker, Tuj1 (Fig. S8C). Reactive astrocytes were generated by treating isolated astrocytes with bacterial lipopolysaccharide (LPS), which induced upregulation of the expression of proinflammatory cytokines including TNF-α, iNOS-2, IL-1β and IL-6 as determined by qPCR (Fig. S8D), confirming astrocyte activation. Exosomes were purified from control and LPS-activated astrocytes using differential centrifugation and the presence of exosomes in pellets confirmed by immunoblotting for CD81, TSG101 and Flotillin1 and by confirming particle diameters using

NTA (Fig. S8E and F). Interestingly, treatment of neurons with varying doses of exosomes isolated from either control or LPS-activated astrocytes inhibited neurite outgrowth (Fig. 6D-G). As tissue culture plastic is much stiffer than the normal *in vivo* environment and can stimulate partial activation of astrocytes (East *et al*, 2009), we next cultured astrocytes in a soft 3D-collagen gel, hereafter referred as 3D-astrocytes. GFAP expression is higher in activated astrocytes (Escartin *et al*, 2021) and accordingly, astrocytes grown on a 2D-plastic surface showed much higher GFAP staining as compared to those cultured in the 3D-collagen gel (Fig. S8G). Moreover, treatment of 3D-astrocytes with LPS, enhanced GFAP expression (Fig. S8H). Next, exosomes were isolated from control and LPS-activated 3D-astrocytes and were confirmed to display typical exosome size using NTA (Fig. S8I-K). Remarkably, exosomes isolated from 3D-astrocytes had no effect on the neurite outgrowth (Fig. 6H and I), whereas exosomes from LPS-activated 3D-astrocytes inhibited the neurite outgrowth (Fig. 6J and K). Thus, our results indicate that while reactive astrocytes inhibit neurite outgrowth, control, unstimulated astrocytes grown in a soft environment do not alter neuronal morphology.

Taken together, these findings suggest that the exosome-induced neurite outgrowth is a unique feature of fibroblast-derived exosomes, and not a general property of exosomes. Collectively, the data supports a model in which exosomes mobilize the autocrine Wnt-PCP signaling in neurons to promote neuronal polarity and axon outgrowth. We suggest a novel mechanism whereby internalized exosomes which co-localize with Wnt ligands, such as Wnt7b, induce relocalization of the core PCP component, Vangl2 from the soma to distal part of the axon and thereby promote axon outgrowth (Fig. 7).

Discussion

In the CNS, external cues including EVs and more specifically exosomes from diverse sources modulate neurite outgrowth, but how fibroblast-derived exosomes act to specifically affect neuronal morphology remains unclear. Here, we show that fibroblast-derived exosomes can mobilize autocrine Wnt-PCP signaling in neurons and thereby promote axon outgrowth and acquisition of a polarized neuronal morphology. We demonstrate that exosomes are internalized via the soma in neurons and can colocalize with endogenous Wnt7b and that exosomes induce relocalization of the core PCP component, Vangl2 to the distal region of the axon. Thus, our work

demonstrates that exosomes can trigger autocrine Wnt-PCP signaling in neurons to promote axon outgrowth.

Exosomes derived from diverse sources harbour the ability to promote axon or dendrite elongation. For instance, exosomes from Schwann cells of the PNS have been shown to promote neurite outgrowth in dorsal root ganglia (DRG) neurons, and exosomes from mesenchymal cells enhance neurite outgrowth in DRG and CNS-derived cortical neurons (Xin *et al.*, 2012; Lopez-Verrilli *et al.*, 2013; Lopez-Verrilli *et al.*, 2016; Zhang *et al.*, 2017). In the case of fibroblasts, exosomes from these cells can promote neurite outgrowth in DRG neurons in normal, uninjured contexts, and can enhance axon regeneration in injured sciatic nerves (Zhao *et al*, 2023). In addition, fibroblasts can promote Schwann cell migration and sorting, both of which are associated with axonal regrowth (Dreesmann *et al*, 2009; Parrinello *et al.*, 2010; van Neerven *et al*, 2013). In our study, we found that fibroblast-derived exosomes can promote axon outgrowth in cortical neurons and that they act through the Wnt-PCP pathway. In contrast, in a prior study, fibroblast-derived exosomes were shown to promote axon regeneration in a Wnt-dependent manner but did so via the mTOR pathway and only in neurons grown in an inhibitory environment (Tassew *et al.*, 2017). Thus exosomes appear to be capable of activating distinct neuronal signaling pathways in growth permissive versus inhibitory contexts. In contrast to fibroblasts, we observed that exosomes derived from primary neurons or unactivated astrocytes had no effect on neurite outgrowth even when used at higher concentrations. Upon damage, activated astrocytes contribute to the inhibitory microenvironment by forming a glial scar at the injury site (Pekny & Pekna, 2014; Liddelow & Barres, 2017; Lee *et al.*, 2022). In line with this, we observed that exosomes derived from LPS-activated astrocytes inhibit neurite outgrowth, which is consistent with a previous report showing that exosomes from Interleukin-1β-activated human primary astrocytes similarly inhibited neurite outgrowth in mouse cortical neurons (You *et al*, 2020). This suggests that the cell type and state of exosome secreting cells determines the axon growth promoting properties of exosomes. Understanding the mechanisms that alter exosome cargos to thereby modulate the effects on neurons is an important area for future investigation.

Core PCP components modulate many aspects of neuronal morphology including neuronal polarization, axon outgrowth, axon guidance and synapse formation (Goodrich, 2008; Davey &

Moens, 2017; Hakanen *et al.*, 2019; Zou, 2020). Our data shows that both of the related PCP components, Pk1 and Pk2 are required for growth of the prospective axon, which is consistent with a recent study showing that Pk2 is necessary for proper neuronal polarity in rat hippocampal neurons (Dorrego-Rivas *et al*, 2022). We also observed that the absence of Pk1 and Pk2 attenuated exosome-induced growth of the longest neurite. Another core PCP component, Vangl2 has been reported to exhibit differential effects in distinct neurons. For instance, downregulation of Vangl2 in commissural neurons using shRNAs inhibited Wnt5a-induced axonal outgrowth (Shafer *et al.*, 2011), whereas hippocampal neurons from Vangl2 conditional-knockout mice exhibited increased basal and Wnt5a-induced axon outgrowth (Dos-Santos Carvalho *et al*, 2020). In our study, we observed that both Vangl1 and Vangl2 are required for basal neurite outgrowth and that only Vangl2 is required for exosome-induced neurite outgrowth. Importantly, exosomes induced relocalization of Vangl2 to the distal part of the axon, further supporting a role for Vangl2 in exosome-mediated axon outgrowth. Although not designated as core PCP components, members of the Smurf E3 ubiquitin ligase family are important regulators of PCP, and can modulate neuronal morphology (Vohra *et al.*, 2007; Narimatsu *et al.*, 2009; Cheng *et al.*, 2011; Kannan *et al.*, 2012). Consistently, we found that both Smurf1 and Smurf2 are required for neurite outgrowth, and that exosome-induced neurite outgrowth is attenuated in Smurf1 and Smurf2 knockout neurons. Taken together, these results demonstrate that exosomes engage key components of the Wnt/PCP pathway to modulate neuritogenesis.

Fzd receptors and Dvls are essential for PCP signaling, but also mediate canonical Wnt/β-catenin signals (van Amerongen *et al.*, 2008). Diverse Fzd receptors have been shown to modulate events that establish neuronal morphology including axonal polarity and growth, axon guidance, dendrite morphogenesis and synaptogenesis (Pascual-Vargas & Salinas, 2021). In particular, Fzd3, 5 and 9 have been reported to be essential for axon outgrowth and guidance (Pascual-Vargas & Salinas, 2021). In embryonic cortical neurons (E15.5-16.5), we observed that Fzd1, 2, 3, 7, 8 and 9 are expressed at varying levels. Of these Fzds, individual knockdown of Fzd1, Fzd3 or Fzd9 attenuated both basal and exosome-induced neurite outgrowth, whereas Fzd7 was only required for neurite outgrowth mediated by exosomes. This indicates that Fzd1, 3 and 9 act in a non-redundant manner and that Fzd7 is specifically required for exosome-mediated effects. Consistently, a non-redundant role for Fzd3 in mediating axon outgrowth and guidance in knockout mouse models has been

described (Hua *et al*, 2013; Hua *et al*, 2014; Qu *et al*, 2014). The cell surface and intracellular distribution of Fzds can be modulated by post-translational modifications such as phosphorylation (Pascual-Vargas & Salinas, 2021). Moreover, in neurons, a distinctive spatiotemporal localization of Fzds in the soma, axon and growth cone during different developmental stages has been observed (Sahores *et al*, 2010; Varela-Nallar *et al*, 2012; Slater *et al*, 2013). This differential localization of Fzds in space and time, due at least in part to changes in post-translational modifications, could be critical for axon formation and outgrowth, and thus may explain the non-redundant role of Fzds during this process. Dvls are shared by PCP and canonical Wnt pathways and have been reported to modulate axon outgrowth and guidance (Gao & Chen, 2010; Sharma *et al.*, 2018). For instance, Dvl2 has been reported to specifically function in PCP signaling (Onishi *et al*, 2013). We observed that cortical neurons express all three Dvls (Dvl1, 2 and 3), but only Dvl2 was required for exosome-induced neurite outgrowth, a process that we have shown requires PCP signaling. Altogether our data indicates a key role for the PCP pathway in regulating neuronal polarization and axon outgrowth that is enhanced by fibroblast-derived exosomes.

In vertebrates, Wnts are required for the activation of PCP signaling and can modulate neuronal morphology (Butler & Wallingford, 2017; Teo & Salinas, 2021; Koca *et al.*, 2022). Our data shows that neuronal Wnt secretion is required for axon formation as chemical inhibition of porcupine or siRNA-mediated knockdown of Wls, both of which block Wnt secretion, prevented axonogenesis. This observation is consistent with a previous report showing that treatment with the porcupine inhibitor, IWP2, inhibits neuronal polarization in hippocampal neurons (Stanganello *et al*, 2019). Moreover, we observed that exosome-induced neurite outgrowth was inhibited upon blocking neuronal Wnt secretion. We showed that cortical neurons express Wnt5a, 5b, 7a and 7b, three of which (Wnt5b, 7a and 7b) are required for the growth of the prospective axon and for enhanced axon elongation induced by exosomes. Intracellular association of Wnts with exosomes is critical for Wnt secretion on exosomes (Routledge & Scholpp, 2019; Gross, 2021; Mittermeier & Virshup, 2022). Consistent with this, we showed that neuronal Wnt7b, the most highly expressed Wnt in E15.5 cortical neurons, can colocalize with the exogenously applied CD81-positive exosomes within the neurons. This suggests the possibility that exosomes internalized by neurons can engage endogenous Wnts in the context of neurite outgrowth. In a prior study in cancer cells, we showed that a similar mechanism occurs, whereby exosomes from fibroblasts acquire Wnt11 when

internalized by breast cancer cells to activate autocrine Wnt-PCP signaling and promote cell motility and formation of protrusions (Luga *et al.*, 2012). Thus, activation of autocrine Wnt-PCP signaling by exosomes might be a conserved mechanism in diverse biological contexts.

Although the fibroblasts used in our study were derived from skin, lung and mouse embryos, and thus do not reside in CNS, the current study identifies a unique and shared potential of fibroblast-derived exosomes, irrespective of the tissue origin, in activating axon outgrowth systems. At the molecular level, we have shown that exosomes induce axon elongation and a polarized neuronal morphology by mobilizing autocrine Wnt-PCP signaling components. As context-dependent effects of exosomes are not well understood, it will be critical to explore the molecular determinants in exosomes that confer context specificity in varying biological functions.

Acknowledgements

We thank Lisa Qiu, Victoria Leon Guerrero, Bruno Sangiorgi and Nadia Zafar for contributions during the early stages of the project. We thank Dr. Sachdev Sidhu for kindly providing Fzd blocking antibody. This work was funded by grants to L.A. from the CIHR (FDN148455) and from the Krembil Foundation.

Competing Interests

The authors declare that they have no competing interests.

Materials and Methods

Mice

Mouse studies were conducted in accordance with the guidelines of the Canadian Council on Animal Care (CCAC) and approved by the University Animal Care Committee, University of Toronto or The Centre for Phenogenomics (TCP), Toronto, Ontario, Canada. Mice were housed in individually ventilated cages with free access to standard animal food and water in a climate-controlled room with a 12 h light/dark cycle. CD1 pregnant females E15-16 were purchased from Charles River.

Prickle1 (Pk1) conditional knockout mice were generated by introducing Pk1 targeting vector (EUCOMM, HTGR03009_Z_6_E08) into G4 embryonic stem (ES) cells by electroporation. ES cell colonies were selected using Neomycin (Invitrogen, 10131027) and genomic DNA was analyzed by southern blotting to identify homologous recombinants. Chimeric embryos were produced, at the Transgenic Core of the TCP facility, by diploid aggregation of in house generated Pk1 or commercially acquired targeted Pk2 (HEPD0638_2_E01 clone C3) ES cells and CD1 embryos. Chimeric mice were crossed with ICRs mice, obtained from TCP, to obtain the F1 heterozygotes, that were then crossed with Flp recombinase mice to remove the neomycin selection cassette. For the Pk1 allele, genomic DNA was digested with NdeI and probed with a Pk1 3′ probe, resulting in a 15.7 kb (wild-type allele) and a 10.4 kb (mutant allele) fragment. For the Pk2 allele, genomic DNA was digested with BstEII, ScaI, NsiI, AvrII, or Bsu36 and probed with a Neo probe to produce targeted bands of 15Kb, 18.5Kb, 17.6 Kb, 9.5Kb or 12.7Kb, respectively. Single floxed mice ($Pk1^{fl/fl}$; $Pk2^{+/+}$ and $Pk1^{+/+}$; $Pk2^{fl/fl}$) were crossed with each other to obtain Pk1/2 double floxed mice ($Pk1^{fl/fl}$; $Pk2^{fl/fl}$). To obtain the brain specific conditional knockout, single floxed mice and double floxed mice were crossed with a Nestin-Cre line, acquired from TCP, to obtain Cre+ ($Pk1^{fl/fl}$;$Pk2^{+/+}$;Cre+, $Pk1^{+/+}$;$Pk2^{fl/fl}$;Cre+, $Pk1^{fl/fl}$;$Pk2^{fl/fl}$;Cre+) and Cre- ($Pk1^{fl/fl}$; $Pk2^{+/+}$;Cre-, $Pk1^{+/+}$;$Pk2^{fl/fl}$;Cre-, $Pk1^{fl/fl}$; $Pk2^{fl/fl}$;Cre-) floxed mice that were subsequently crossed with each other to obtain the various genotype combinations. For genotyping, genomic DNA from 2 mm E16.5 tail piece was isolated and then subjected to PCR using primers listed in Table S1. Loss of Pk1/2 expression was confirmed in brain sections from $Pk1^{fl/fl}$; $Pk2^{fl/fl}$;Nestin-Cre+ mice by immunostaining with Pk1/2 antibodies (Table S2), followed by confocal microscopy.

Heterozygous Vangl2$^{Lp/+}$ (Vangl2^{S464N}) mice (Strong & Hollander, 1949), obtained from Jackson Labs (#000220), were kindly provided by Dr. Helen McNeil (Lunenfeld-Tanenbaum Research Institute, Mount Sinai Hospital, Toronto, Ontario, Canada) and crossed with each other to obtain homozygous mutants (Vangl2$^{Lp/Lp}$). Smurf1/2 heterozygous mice (Smurf1$^{+/-}$; Smurf2$^{+/-}$) were generated previously (Narimatsu *et al.*, 2009), and crossed with each other to generate single knockout (Smurf1$^{-/-}$ or Smurf2$^{-/-}$) embryos.

Isolation, culturing and transfection of mouse cortical neurons

Primary cortical neurons were isolated from mouse embryos E15.5-16.5 as previously described (Christova *et al*, 2023). Briefly, brains were harvested and placed in ice-cold HBSS (Gibco) and cerebral cortices were dissected. Cortices were digested in 0.25 % Trypsin-EDTA (Gibco, 25200056) at 37°C followed by trypsin inactivation by adding Dulbecco's Modified Eagle Medium (DMEM) (Gibco, 11995-065) containing 10% FBS (Gibco, 12483-020). After further mechanical dissociation, neurons were seeded at a density of 30000 cells/well for regular experiments or 125,000 cells/well for transfection experiments in 4-well chamber slides (Lab-Tek II, 155382) coated with poly-L-lysine (20 µg/mL, Sigma, P1399) and laminin (2 µg/mL, Corning, 354232). Neurons were cultured at 37°C and 5% CO_2 in Neurobasal medium (Gibco, 21103-049) supplemented with 2% B-27 (Gibco, 17504-044), 0.5% N-2 (Gibco, 17502-048), 2 mM GlutaMAX™ (Gibco, 35050-061) and 0.5% penicillin/streptomycin (Gibco, 15140-122).

For transfections, dissociated neurons were electroporated with cDNA (2 µg) or siRNA (Table S1) using an Amaxa nucleofector (program-005, Lonza) and mouse neuron nucleofector™ kit (VPG-1001, Lonza) according to the manufacturer's instructions. Briefly, neurons (4-5 × 10^6) were electroporated with a mix of 2 µM siGENOME SMARTpool siRNAs (Dharmacon) and 2 µg of enhanced green fluorescent protein (eGFP) as a transfection reporter. Media was replaced 4 h after seeding. All DNAs were prepared using Endotoxin- Free Maxi-prep kit (Qiagen).

Mammalian cell culture and transfection

L cells (CRL-2648), Human Dermal fibroblasts (HDFn) (PCS-201-010™), BJ cells (CRL-2522™) and MDA-MB-231 cells were purchased from ATCC, normal Human Lung Fibroblasts

(NHLF) were purchased from Lonza (CC-2512) and mouse embryonic fibroblasts (MEFs) were acquired from the TCP facility. MDA-MB-231 cells were cultured in Roswell Park Memorial Institute (RPMI) 1640 medium containing 5% FBS while all other lines were cultured in DMEM containing 10% FBS. Cell lines were routinely tested for mycoplasma contamination using MycoAlert™ Plus reagent (Lonza, LT07-703).

For siRNA transfections, L cells were (1×10^6) were transfected with 40 nM siGENOME SMARTpool siRNAs (Dharmacon) using Lipofectamine™ RNAiMAX reagent (Invitrogen, 13778075) according to manufacturer's protocols. For cDNA transfection of MDA-MB-231 cells, plasmids (2 µg) were delivered using Lipofectamine® 3000 (Invitrogen, L3000-001) according to manufacturer's instructions. The Wnt7b construct was generated using Gateway system (Life Technologies) by transfer from an entry clone into a C-terminal HA-tagged pCMV5-based destination vector.

Primary Astrocyte Cultures

Dissociated primary astrocytes were isolated from the cortices of CD1 mouse post-natal (P1-P4) pups as previously published (Schildge *et al*, 2013). Dissociated cells were cultured in DMEM supplemented with heat inactivated 10% FBS and 1% penicillin/streptomycin in 75 cm^2 flasks (Corning, 430720U) coated with poly-D-lysine (50 µg/mL, Sigma, P7280). Media was changed after 24 h of initial seeding, and every 2 days thereafter. Cultures were grown for 8 days. and then shaken at 120 rpm overnight to remove microglia and less adherent cells. Cells were then washed, trypsinized and these astrocyte enriched cultures were used for subsequent experiments.

For 3D cultures, astrocytes were seeded in a gel containing type-I rat tail collagen (Ibidi, 50201), prepared according to the manufacturer's protocol. Briefly, 10% minimum essential media (MEM, Gibco, 11430-030), 1% GlutaMAX™ and collagen (2 mg/mL) were mixed on ice and neutralized using 1M NaOH. Subsequently, DMEM containing cells was gently added to the gel mixture resulting in a cell density of 2×10^6 cells/mL of gel mixture. Gel mixture was transferred to either 6-well plates (2.5 mL/well) for exosome isolation or in chamber slides (700 µL/well) for immunofluorescence microscopy. The liquid gel mixture was placed at 37°C and 5% CO_2 for 30

minutes to solidify and then fresh DMEM containing heat inactivated 10% FBS and 1% penicillin/streptomycin was added.

Preparation of Conditioned Media

Fibroblasts (0.5×10^6) were seeded in a 100 mm dish and grown to confluency. Cells were washed with DMEM and incubated with DMEM either without FBS (L cells) or exosome free 10% FBS (for NHLF, HDFn, BJ, MEFs) (Gibco). After 3-4 days, conditioned media (CM) was collected, centrifuged at 300 x g to remove cells and stored at 4 °C for up to eight weeks. CM from neurons was prepared from primary cortical neurons (4×10^6 cells) seeded in a 100 mm dish and cultured in a serum free complete medium. On day 4, 25% of freshly made complete medium supplemented with 5 µM cytosine β-d-arabinofuranoside (Sigma, C1768) was added and CM was collected on day 8. For 2D astrocytes, enriched primary astrocytes cells were seeded in p75 flasks and cultured in DMEM supplemented with heat inactivated exosome free 10% FBS. Cultures were grown to confluency, and the CM was collected after 6 days. For 3D astrocytes cultures in collagen gel, enriched primary astrocytes were seeded in 6 well plate and CM was collected after 6 days.

Exosome purification by differential centrifugation

Conditioned-media (CM) (50 mL) was collected from fibroblasts, neurons or astrocytes and centrifuged at 300 x g for 5 min and at 2000 x g for 20 min to remove cells and large debris, respectively. Supernatants were then centrifuged at 10,000 x g for 30 min to remove apoptotic bodies and large vesicles. The resulting supernatants were filtered through a 0.2 µm filter (Thermo Fisher Scientific, 568-0020) and ultracentrifuged at 100,000 x g (Type 70 Ti rotor, Beckman Coulter) for 2 h using 25 × 89 mm polycarbonate tubes (Beckman Coulter, 355618). Pellets were resuspended in 500 µL of sterile phosphate-buffered saline (PBS) and diluted with 7.5 mL of PBS. Diluted pellets were ultracentrifuged at 100,000 x g (Type 70.1 Ti rotor, Beckman Coulter) for 2 h using 16 × 76 mm polycarbonate tubes (Beckman Coulter, 355603). The resulting pellets were resuspended in 250 µL of sterile PBS, aliquoted and stored at -80°C.

Exosome purification using iodixanol density gradient

A discontinuous iodixanol gradient, prepared by diluting 60% iodixanol (Optiprep™, Sigma, D1556) with 0.25 M sucrose / 10 mM Tris, pH 7.4, was used to further purify the exosome pellets

(100,000 x g). Exosome pellet, resuspended in 500 μL of PBS, was overlaid on top of the discontinuous gradient (40%, 20%, 10% and 5%; 3 mL each, but 2.5 mL for 5%) and ultracentrifuged at 100,000 x g (SW 40 Ti rotor, Beckman Coulter) for 16 h using ultra-clear tubes (Beckman Coulter, 344060). Twelve fractions of 1 mL each were collected manually from the top. Fractions were washed by diluting with 7 mL of PBS and ultracentrifuged at 100,000 x g (Type 70.1 Ti rotor, Beckman Coulter) for 2 h. The resulting pellets were resuspended in 250 μL of sterile PBS and stored at -80°C.

Exosome purification by size exclusion chromatography

Exosome pellets (100,000 x g) were also purified using qEV original size exclusion column with a pore size of 70 nm (Izon science, 1001683) according to manufacturer's protocol with minor modifications. Briefly, the column was equilibrated with 30 mL of PBS and exosome pellet, resuspended in 500 μL of PBS, was overlaid on qEV column followed by elution with PBS. Fractions of 500 μL were collected and analyzed for particle and protein concentration using NTA and Bradford assay, respectively.

Exosome purification by Exo-spin™ precipitation

Exosomes from 3D-astrocytes were purified using Exo-spin™ purification kit (Cell Guidance Systems) according to manufacturer's instructions. Briefly, CM was precleared by sequential centrifugations at 300 x g, 2000 x g and 10,000 x g. Supernatants were mixed with the precipitation buffer and incubated overnight at 4°C. Samples were centrifuged at 10,000 x g for 30 min and pellets were re-suspended in 200 μL of PBS. Samples were further purified using provided size exclusion columns and exosomes were eluted in 200 μL of PBS.

Nanoparticle Tracking Analysis

The number of particles were measured using ZetaView® PMX 110 device (Particle Metrix GmbH, Germany). The measurements were taken at all 11 different positions with camera sensitivity set to 90 and shutter speed at 45 using the ZetaView software (version 8.03.08). The video quality was set to medium, and the data was analysed using the ZetaView analysis software (version 8.02.31) with the following post-acquisition parameters: minimum size 10, maximum size 1000, and minimum brightness 20.

Exosome internalization assay

For exosome internalization assays, 50 mL of media was collected from L cells stably transfected with either CD81-EYFP or CD81-pLVX as a control (Luga *et al.*, 2012). CM was centrifuged at 300 x g for 5 min and at 2000 x g for 20 min to remove cells and large debris, respectively. Supernatants were concentrated 10-fold using a 10 kDa MWCO filter (Amicon® Ultra-15, UFC901008). Neurons were seeded in 8 well Ibidi chambers and treated with 10X CM for 29 h or 30 min, prior to fixation, immunostaining and imaging using confocal microscopy.

Neurite outgrowth assay in a microfluidic chamber

Two compartment microfluidic chambers containing a 150 µm microgroove were purchased from Xona Microfluidics (XC150). Chambers were prepared for seeding neurons according to manufacturer's instructions with a few modifications. Briefly, chambers were treated with a pre-coat solution and subsequently coated with poly-L-lysine (20 µg/mL) and laminin (2 µg/mL). Cortical neurons (50,000 cells) were seeded in one well in an initial volume of 20 µL and allowed to adhere for 5 min at 37°C and 5% CO_2. Complete Neurobasal medium was added to all the wells and neurons cultured for 5 days until axons crossed the microgroove and emerged in the distal chamber. Exosomes (5 µg/mL) were added either to the somal side or axonal sides on day 5 for 24 h prior to fixation and immunostaining.

RT and qPCR

For neurons and astrocytes, total RNA was extracted using the Norgen Single-Cell RNA Purification Kit (Norgen, 51800). For other cells, total RNA was extracted using PureLink RNA Mini Kit (Life Technologies, 12183025). Complementary DNA was synthesized using 35 to 200 ng of purified RNA using oligo-dT primers and M-MLV Reverse Transcriptase (Invitrogen, 28025-013). Real-time qPCR was performed using SYBR™ Green PCR Master Mix (Applied Biosciences, 4309155) on the QuantStudio 6 Flex System (Applied Biosciences). Relative gene expression was quantified using the ΔΔCt method and normalized to glyceraldehyde-3-phosphate dehydrogenase (Gapdh). Primers used are listed in the Supplementary Table S3.

Immunofluorescence microscopy and immunoblotting

Neurons and astrocytes were fixed in 4% paraformaldehyde as previously described (Christova *et al.*, 2023). Briefly, cells were permeabilized with 0.2% Triton/PBS, washed with PBS, and blocked at room temperature for 1 h with 3% Bovine Serum Albumin (BSA)/PBS. Cells were incubated with primary antibodies for 2 h at room temperature or overnight at 4°C, washed 3 times with PBS, and incubated with secondary antibodies for 2 h at room temperature. Cells were washed with PBS and stored in PBS or in Ibidi mounting medium prior to imaging. For epifluorescence microscopy, images were acquired using the 40X Plan-NEOFLUAR objective of Zeiss Axiovert 200 M epifluorescence microscope. For confocal microscopy, images were acquired using Zeiss AXIO Observer Z1 microscope equipped with Zen Blue software, a spinning disc confocal scanner (CSU-X1, Yokogawa) and a CCD camera (Axiocam 506 mono) with following objectives: Plan-Apochromat 20x/0.8 M27 air, Plan-Apochromat 40x/1.4 Oil DIC and Plan-Apochromat 63x/1.4 Oil DIC M27. Some confocal images were acquired using Nikon ECLIPSE Ti2 inverted microscope equipped with LUA-S laser unit and NIS-Elements software (from Nikon) with following objectives: Nikon-N Apo-LWD 40X/1.15 WI and Nikon-N Apo-LWD 20X/0.95 WI. All images were acquired in a random fashion.

For immunoblotting, cells were lysed in lysis buffer (50 mM Tris-HCl, 150 mM NaCl, 1 mM EDTA, 0.5% Triton X-100, 1 mM DTT containing protease and phosphatase inhibitors) (Bao *et al*, 2012). Protein concentration was determined using Bradford reagent (BIORAD). Proteins from cell lysates (1-20 μg) and exosomes (1-10 μg) were separated on an SDS-PAGE gel and analyzed by immunoblotting as described previously (Heidary Arash *et al*, 2014).

Electron microscopy

Exosomes were visualized using Talos L120C transmission electron microscope (TEM) (Thermo Scientific) in the Microscopy Imaging Laboratory, University of Toronto, Canada. Exosome samples were frozen on TEM grids (Quantifoil R2,2 300 mesh, EMS) that were charged for 30 seconds with a Pelco EasiGlow glow discharge cleaning system (Ted Pella). Samples (4 μL) were deposited onto the grid and the grid was blotted and plunge frozen using a Vitrobot IV (FEI).

Images were taken using 120kV at magnifications 28000x and 57000x, corresponding to a pixel size of 510 and 249 pm respectively. Images were collected at a defocus of -4 to -1.5 microns using the TEM Image and Analysis (TIA) software.

Quantification

For Tuj1 stained neurons, the length of all neurites (including the longest neurite, a prospective axon, and dendrites, all other neurites excluding the longest neurite) were quantified using Volocity software (Quorum Technologies Inc, Canada). In MAP2 and Tau-1 experiments, neurons were classified into two groups: only MAP2-positive minor neurites or minor neurites and a single Tau-1-positive axon displaying medial-to-distal localization of the Tau-1.

For Vangl2 localization, neurons were classified into three groups (proximal, distal, or equal) Vangl2 distribution was determined by visual analysis. For exosome and Wnt7b co-localization, neurons were identified using Tuj1 as reference channel and the Pearson's colocalization coefficient for GFP (exosomes) and Wnt7b was determined using Nikon NIS-Elements software (Version 5.41.00).

Statistical Analyses

The data for the axon length and longest neurite length is plotted as the average of the median ± SEM from 90-120 neurons per condition in 3 independent experiments. The data was analyzed statistically using an unpaired t-test for comparing two groups or one-way ANOVA with Dunnetts post-test for multiple comparisons to a single control group, or two-way ANOVA with Tukey's post-test for multiple comparisons to control and between the samples, as indicated in the figure legends. All statistics were done in GraphPad PRISM 9 (GraphPad software Inc. La Jolla, CA). Statistical significance: *$p<0.05$, **$p<0.01$, ***$p<0.001$.

References

Arimura N, Kaibuchi K (2007) Neuronal polarity: from extracellular signals to intracellular mechanisms. *Nat Rev Neurosci* 8: 194-205.

Bahram Sangani N, Gomes AR, Curfs LMG, Reutelingsperger CP (2021) The role of Extracellular Vesicles during CNS development. *Prog Neurobiol* 205: 102124.

Banziger C, Soldini D, Schutt C, Zipperlen P, Hausmann G, Basler K (2006) Wntless, a conserved membrane protein dedicated to the secretion of Wnt proteins from signaling cells. *Cell* 125: 509-522.

Bao R, Christova T, Song S, Angers S, Yan X, Attisano L (2012) Inhibition of tankyrases induces Axin stabilization and blocks Wnt signalling in breast cancer cells. *PLoS One* 7: e48670.

Belotti E, Puvirajesinghe TM, Audebert S, Baudelet E, Camoin L, Pierres M, Lasvaux L, Ferracci G, Montcouquiol M, Borg JP (2012) Molecular characterisation of endogenous Vangl2/Vangl1 heteromeric protein complexes. *PLoS One* 7: e46213.

Bonansco C, Cerpa W, Inestrosa NC (2022) How Are Synapses Born? A Functional and Molecular View of the Role of the Wnt Signaling Pathway. *Int J Mol Sci* 24: 708.

Bradke F (2022) Mechanisms of Axon Growth and Regeneration: Moving between Development and Disease. *J Neurosci* 42: 8393-8405.

Butler MT, Wallingford JB (2017) Planar cell polarity in development and disease. *Nat Rev Mol Cell Biol* 18: 375-388.

Buzas EI (2023) The roles of extracellular vesicles in the immune system. *Nat Rev Immunol* 23: 236-250.

Chen B, Dodge ME, Tang W, Lu J, Ma Z, Fan CW, Wei S, Hao W, Kilgore J, Williams NS *et al* (2009) Small molecule-mediated disruption of Wnt-dependent signaling in tissue regeneration and cancer. *Nat Chem Biol* 5: 100-107.

Cheng PL, Lu H, Shelly M, Gao H, Poo MM (2011) Phosphorylation of E3 ligase Smurf1 switches its substrate preference in support of axon development. *Neuron* 69: 231-243.

Chivet M, Javalet C, Hemming F, Pernet-Gallay K, Laulagnier K, Fraboulet S, Sadoul R (2013) Exosomes as a novel way of interneuronal communication. *Biochem Soc Trans* 41: 241-244.

Christova T, Ho SK, Liu Y, Gill M, Attisano L (2023) LTK and ALK promote neuronal polarity and cortical migration by inhibiting IGF1R activity. *EMBO Rep* 24: e56937.

Clarke LE, Barres BA (2013) Emerging roles of astrocytes in neural circuit development. *Nat Rev Neurosci* 14: 311-321.

Clarke LE, Liddelow SA, Chakraborty C, Munch AE, Heiman M, Barres BA (2018) Normal aging induces A1-like astrocyte reactivity. *Proc Natl Acad Sci U S A* 115: E1896-E1905.

Colombo M, Raposo G, Thery C (2014) Biogenesis, secretion, and intercellular interactions of exosomes and other extracellular vesicles. *Annu Rev Cell Dev Biol* 30: 255-289.

Davey CF, Moens CB (2017) Planar cell polarity in moving cells: think globally, act locally. *Development* 144: 187-200.

Devenport D (2016) Tissue morphodynamics: Translating planar polarity cues into polarized cell behaviors. *Semin Cell Dev Biol* 55: 99-110.

Dorrego-Rivas A, Ezan J, Moreau MM, Poirault-Chassac S, Aubailly N, De Neve J, Blanchard C, Castets F, Freal A, Battefeld A *et al* (2022) The core PCP protein Prickle2 regulates axon number and AIS maturation by binding to AnkG and modulating microtubule bundling. *Sci Adv* 8: eabo6333.

Dos-Santos Carvalho S, Moreau MM, Hien YE, Garcia M, Aubailly N, Henderson DJ, Studer V, Sans N, Thoumine O, Montcouquiol M (2020) Vangl2 acts at the interface between actin and N-cadherin to modulate mammalian neuronal outgrowth. *Elife* 9: e51822.

Dotti CG, Sullivan CA, Banker GA (1988) The establishment of polarity by hippocampal neurons in culture. *J Neurosci* 8: 1454-1468.

Dreesmann L, Mittnacht U, Lietz M, Schlosshauer B (2009) Nerve fibroblast impact on Schwann cell behavior. *Eur J Cell Biol* 88: 285-300.

Dreyer CA, VanderVorst K, Carraway KL, 3rd (2022) Vangl as a Master Scaffold for Wnt/Planar Cell Polarity Signaling in Development and Disease. *Front Cell Dev Biol* 10: 887100.

East E, Golding JP, Phillips JB (2009) A versatile 3D culture model facilitates monitoring of astrocytes undergoing reactive gliosis. *J Tissue Eng Regen Med* 3: 634-646.

Escartin C, Galea E, Lakatos A, O'Callaghan JP, Petzold GC, Serrano-Pozo A, Steinhauser C, Volterra A, Carmignoto G, Agarwal A *et al* (2021) Reactive astrocyte nomenclature, definitions, and future directions. *Nat Neurosci* 24: 312-325.

Fan Y, Chen Z, Zhang M (2022) Role of exosomes in the pathogenesis, diagnosis, and treatment of central nervous system diseases. *J Transl Med* 20: 291.

Gao C, Chen YG (2010) Dishevelled: The hub of Wnt signaling. *Cell Signal* 22: 717-727.

Gassama Y, Favereaux A (2021) Emerging Roles of Extracellular Vesicles in the Central Nervous System: Physiology, Pathology, and Therapeutic Perspectives. *Front Cell Neurosci* 15: 626043.

Goodrich LV (2008) The plane facts of PCP in the CNS. *Neuron* 60: 9-16.

Goodrich LV, Strutt D (2011) Principles of planar polarity in animal development. *Development* 138: 1877-1892.

Gross JC (2021) Extracellular WNTs: Trafficking, Exosomes, and Ligand-Receptor Interaction. *Handb Exp Pharmacol* 269: 29-43.

Hakanen J, Ruiz-Reig N, Tissir F (2019) Linking Cell Polarity to Cortical Development and Malformations. *Front Cell Neurosci* 13: 244.

Heidary Arash E, Song KM, Song S, Shiban A, Attisano L (2014) Arhgef7 promotes activation of the Hippo pathway core kinase Lats. *EMBO J* 33: 2997-3011.

Hua ZL, Jeon S, Caterina MJ, Nathans J (2014) Frizzled3 is required for the development of multiple axon tracts in the mouse central nervous system. *Proc Natl Acad Sci U S A* 111: E3005-3014.

Hua ZL, Smallwood PM, Nathans J (2013) Frizzled3 controls axonal development in distinct populations of cranial and spinal motor neurons. *Elife* 2: e01482.

Jones C, Chen P (2007) Planar cell polarity signaling in vertebrates. *Bioessays* 29: 120-132.

Kannan M, Lee SJ, Schwedhelm-Domeyer N, Stegmuller J (2012) The E3 ligase Cdh1-anaphase promoting complex operates upstream of the E3 ligase Smurf1 in the control of axon growth. *Development* 139: 3600-3612.

Kibar Z, Vogan KJ, Groulx N, Justice MJ, Underhill DA, Gros P (2001) Ltap, a mammalian homolog of Drosophila Strabismus/Van Gogh, is altered in the mouse neural tube mutant Loop-tail. *Nat Genet* 28: 251-255.

Koca Y, Collu GM, Mlodzik M (2022) Wnt-frizzled planar cell polarity signaling in the regulation of cell motility. *Curr Top Dev Biol* 150: 255-297.

Lee HG, Wheeler MA, Quintana FJ (2022) Function and therapeutic value of astrocytes in neurological diseases. *Nat Rev Drug Discov* 21: 339-358.

Liddelow SA, Barres BA (2017) Reactive Astrocytes: Production, Function, and Therapeutic Potential. *Immunity* 46: 957-967.

Liu J, Pan S, Hsieh MH, Ng N, Sun F, Wang T, Kasibhatla S, Schuller AG, Li AG, Cheng D *et al* (2013) Targeting Wnt-driven cancer through the inhibition of Porcupine by LGK974. *Proc Natl Acad Sci U S A* 110: 20224-20229.

Lopez-Verrilli MA, Caviedes A, Cabrera A, Sandoval S, Wyneken U, Khoury M (2016) Mesenchymal stem cell-derived exosomes from different sources selectively promote neuritic outgrowth. *Neuroscience* 320: 129-139.

Lopez-Verrilli MA, Picou F, Court FA (2013) Schwann cell-derived exosomes enhance axonal regeneration in the peripheral nervous system. *Glia* 61: 1795-1806.

Luga V, Zhang L, Viloria-Petit AM, Ogunjimi AA, Inanlou MR, Chiu E, Buchanan M, Hosein AN, Basik M, Wrana JL (2012) Exosomes mediate stromal mobilization of autocrine Wnt-PCP signaling in breast cancer cell migration. *Cell* 151: 1542-1556.

MacDonald BT, He X (2012) Frizzled and LRP5/6 receptors for Wnt/beta-catenin signaling. *Cold Spring Harb Perspect Biol* 4: a007880.

Merte J, Jensen D, Wright K, Sarsfield S, Wang Y, Schekman R, Ginty DD (2010) Sec24b selectively sorts Vangl2 to regulate planar cell polarity during neural tube closure. *Nat Cell Biol* 12: 41-46.

Mikels AJ, Nusse R (2006) Wnts as ligands: processing, secretion and reception. *Oncogene* 25: 7461-7468.

Mittermeier L, Virshup DM (2022) An itch for things remote: The journey of Wnts. *Curr Top Dev Biol* 150: 91-128.

Mlodzik M (2016) The Dishevelled Protein Family: Still Rather a Mystery After Over 20 Years of Molecular Studies. *Curr Top Dev Biol* 117: 75-91.

Montcouquiol M, Kelley MW (2020) Development and Patterning of the Cochlea: From Convergent Extension to Planar Polarity. *Cold Spring Harb Perspect Med* 10: a033266.

Murdoch JN, Doudney K, Paternotte C, Copp AJ, Stanier P (2001) Severe neural tube defects in the loop-tail mouse result from mutation of Lpp1, a novel gene involved in floor plate specification. *Hum Mol Genet* 10: 2593-2601.

Namba T, Funahashi Y, Nakamuta S, Xu C, Takano T, Kaibuchi K (2015) Extracellular and Intracellular Signaling for Neuronal Polarity. *Physiol Rev* 95: 995-1024.

Narimatsu M, Bose R, Pye M, Zhang L, Miller B, Ching P, Sakuma R, Luga V, Roncari L, Attisano L *et al* (2009) Regulation of planar cell polarity by Smurf ubiquitin ligases. *Cell* 137: 295-307.

Niehrs C (2012) The complex world of WNT receptor signalling. *Nat Rev Mol Cell Biol* 13: 767-779.

Nusse R, Clevers H (2017) Wnt/beta-Catenin Signaling, Disease, and Emerging Therapeutic Modalities. *Cell* 169: 985-999.

Onishi K, Shafer B, Lo C, Tissir F, Goffinet AM, Zou Y (2013) Antagonistic functions of Dishevelleds regulate Frizzled3 endocytosis via filopodia tips in Wnt-mediated growth cone guidance. *J Neurosci* 33: 19071-19085.

Parrinello S, Napoli I, Ribeiro S, Wingfield Digby P, Fedorova M, Parkinson DB, Doddrell RD, Nakayama M, Adams RH, Lloyd AC (2010) EphB signaling directs peripheral nerve regeneration through Sox2-dependent Schwann cell sorting. *Cell* 143: 145-155.

Pascual-Vargas P, Salinas PC (2021) A Role for Frizzled and Their Post-Translational Modifications in the Mammalian Central Nervous System. *Front Cell Dev Biol* 9: 692888.

Pavlovic Z, Adams JJ, Blazer LL, Gakhal AK, Jarvik N, Steinhart Z, Robitaille M, Mascall K, Pan J, Angers S *et al* (2018) A synthetic anti-Frizzled antibody engineered for broadened specificity exhibits enhanced anti-tumor properties. *MAbs* 10: 1157-1167.

Pegtel DM, Gould SJ (2019) Exosomes. *Annu Rev Biochem* 88: 487-514.

Pekny M, Pekna M (2014) Astrocyte reactivity and reactive astrogliosis: costs and benefits. *Physiol Rev* 94: 1077-1098.

Qu Y, Huang Y, Feng J, Alvarez-Bolado G, Grove EA, Yang Y, Tissir F, Zhou L, Goffinet AM (2014) Genetic evidence that Celsr3 and Celsr2, together with Fzd3, regulate forebrain wiring in a Vangl-independent manner. *Proc Natl Acad Sci U S A* 111: E2996-3004.

Radaszkiewicz KA, Sulcova M, Kohoutkova E, Harnos J (2023) The role of prickle proteins in vertebrate development and pathology. *Mol Cell Biochem*.

Rim EY, Clevers H, Nusse R (2022) The Wnt Pathway: From Signaling Mechanisms to Synthetic Modulators. *Annu Rev Biochem* 91: 571-598.

Routledge D, Scholpp S (2019) Mechanisms of intercellular Wnt transport. *Development* 146: dev176073.

Sahai E, Garcia-Medina R, Pouyssegur J, Vial E (2007) Smurf1 regulates tumor cell plasticity and motility through degradation of RhoA leading to localized inhibition of contractility. *J Cell Biol* 176: 35-42.

Sahores M, Gibb A, Salinas PC (2010) Frizzled-5, a receptor for the synaptic organizer Wnt7a, regulates activity-mediated synaptogenesis. *Development* 137: 2215-2225.

Salinas PC (2012) Wnt signaling in the vertebrate central nervous system: from axon guidance to synaptic function. *Cold Spring Harb Perspect Biol* 4: a008003.

Schelski M, Bradke F (2017) Neuronal polarization: From spatiotemporal signaling to cytoskeletal dynamics. *Mol Cell Neurosci* 84: 11-28.

Schildge S, Bohrer C, Beck K, Schachtrup C (2013) Isolation and culture of mouse cortical astrocytes. *J Vis Exp*: 50079.

Shafer B, Onishi K, Lo C, Colakoglu G, Zou Y (2011) Vangl2 promotes Wnt/planar cell polarity-like signaling by antagonizing Dvl1-mediated feedback inhibition in growth cone guidance. *Dev Cell* 20: 177-191.

Sharma M, Castro-Piedras I, Simmons GE, Jr., Pruitt K (2018) Dishevelled: A masterful conductor of complex Wnt signals. *Cell Signal* 47: 52-64.

Slater PG, Ramirez VT, Gonzalez-Billault C, Varela-Nallar L, Inestrosa NC (2013) Frizzled-5 receptor is involved in neuronal polarity and morphogenesis of hippocampal neurons. *PLoS One* 8: e78892.

Stanganello E, Zahavi EE, Burute M, Smits J, Jordens I, Maurice MM, Kapitein LC, Hoogenraad CC (2019) Wnt Signaling Directs Neuronal Polarity and Axonal Growth. *iScience* 13: 318-327.

Steinhart Z, Angers S (2018) Wnt signaling in development and tissue homeostasis. *Development* 145: dev146589.

Strong LC, Hollander WF (1949) HEREDITARY LOOP-TAIL IN THE HOUSE MOUSE: Accompanied by Imperforate Vagina and with Lethal Craniorachischisis When Homozygous. *J Hered* 40: 329-334.

Takada R, Satomi Y, Kurata T, Ueno N, Norioka S, Kondoh H, Takao T, Takada S (2006) Monounsaturated fatty acid modification of Wnt protein: its role in Wnt secretion. *Dev Cell* 11: 791-801.

Takano T, Funahashi Y, Kaibuchi K (2019) Neuronal Polarity: Positive and Negative Feedback Signals. *Front Cell Dev Biol* 7: 69.

Tao H, Manak JR, Sowers L, Mei X, Kiyonari H, Abe T, Dahdaleh NS, Yang T, Wu S, Chen S *et al* (2011) Mutations in prickle orthologs cause seizures in flies, mice, and humans. *Am J Hum Genet* 88: 138-149.

Tao H, Suzuki M, Kiyonari H, Abe T, Sasaoka T, Ueno N (2009) Mouse prickle1, the homolog of a PCP gene, is essential for epiblast apical-basal polarity. *Proc Natl Acad Sci U S A* 106: 14426-14431.

Tao Y, Mis M, Blazer L, Ustav MJ, Steinhart Z, Chidiac R, Kubarakos E, O'Brien S, Wang X, Jarvik N *et al* (2019) Tailored tetravalent antibodies potently and specifically activate Wnt/Frizzled pathways in cells, organoids and mice. *Elife* 8: e46134.

Tassew NG, Charish J, Shabanzadeh AP, Luga V, Harada H, Farhani N, D'Onofrio P, Choi B, Ellabban A, Nickerson PEB *et al* (2017) Exosomes Mediate Mobilization of Autocrine Wnt10b to Promote Axonal Regeneration in the Injured CNS. *Cell Rep* 20: 99-111.

Taylor AM, Blurton-Jones M, Rhee SW, Cribbs DH, Cotman CW, Jeon NL (2005) A microfluidic culture platform for CNS axonal injury, regeneration and transport. *Nat Methods* 2: 599-605.

Teo S, Salinas PC (2021) Wnt-Frizzled Signaling Regulates Activity-Mediated Synapse Formation. *Front Mol Neurosci* 14: 683035.

Thery C, Witwer KW, Aikawa E, Alcaraz MJ, Anderson JD, Andriantsitohaina R, Antoniou A, Arab T, Archer F, Atkin-Smith GK *et al* (2018) Minimal information for studies of extracellular vesicles 2018 (MISEV2018): a position statement of the International Society for Extracellular Vesicles and update of the MISEV2014 guidelines. *J Extracell Vesicles* 7: 1535750.

Torban E, Wang HJ, Patenaude AM, Riccomagno M, Daniels E, Epstein D, Gros P (2007) Tissue, cellular and sub-cellular localization of the Vangl2 protein during embryonic development: effect of the Lp mutation. *Gene Expr Patterns* 7: 346-354.

van Amerongen R, Mikels A, Nusse R (2008) Alternative wnt signaling is initiated by distinct receptors. *Sci Signal* 1: re9.

van Neerven SG, Pannaye P, Bozkurt A, Van Nieuwenhoven F, Joosten E, Hermans E, Taccola G, Deumens R (2013) Schwann cell migration and neurite outgrowth are influenced by media conditioned by epineurial fibroblasts. *Neuroscience* 252: 144-153.

van Niel G, Carter DRF, Clayton A, Lambert DW, Raposo G, Vader P (2022) Challenges and directions in studying cell-cell communication by extracellular vesicles. *Nat Rev Mol Cell Biol* 23: 369-382.

Varela-Nallar L, Ramirez VT, Gonzalez-Billault C, Inestrosa NC (2012) Frizzled receptors in neurons: from growth cones to the synapse. *Cytoskeleton (Hoboken)* 69: 528-534.

Vohra BP, Fu M, Heuckeroth RO (2007) Protein kinase Czeta and glycogen synthase kinase-3beta control neuronal polarity in developing rodent enteric neurons, whereas SMAD specific E3 ubiquitin protein ligase 1 promotes neurite growth but does not influence polarity. *J Neurosci* 27: 9458-9468.

Wallingford JB (2012) Planar cell polarity and the developmental control of cell behavior in vertebrate embryos. *Annu Rev Cell Dev Biol* 28: 627-653.

Wang HR, Zhang Y, Ozdamar B, Ogunjimi AA, Alexandrova E, Thomsen GH, Wrana JL (2003) Regulation of cell polarity and protrusion formation by targeting RhoA for degradation. *Science* 302: 1775-1779.

Wang M, Marco P, Capra V, Kibar Z (2019) Update on the Role of the Non-Canonical Wnt/Planar Cell Polarity Pathway in Neural Tube Defects. *Cells* 8: 1198.

Wang Y, Chang H, Rattner A, Nathans J (2016) Frizzled Receptors in Development and Disease. *Curr Top Dev Biol* 117: 113-139.

Webber J, Clayton A (2013) How pure are your vesicles? *J Extracell Vesicles* 2: 19861.

Willert K, Nusse R (2012) Wnt proteins. *Cold Spring Harb Perspect Biol* 4: a007864.

Xin H, Li Y, Buller B, Katakowski M, Zhang Y, Wang X, Shang X, Zhang ZG, Chopp M (2012) Exosome-mediated transfer of miR-133b from multipotent mesenchymal stromal cells to neural cells contributes to neurite outgrowth. *Stem Cells* 30: 1556-1564.

Yang Y, Mlodzik M (2015) Wnt-Frizzled/planar cell polarity signaling: cellular orientation by facing the wind (Wnt). *Annu Rev Cell Dev Biol* 31: 623-646.

Yates AG, Pink RC, Erdbrugger U, Siljander PR, Dellar ER, Pantazi P, Akbar N, Cooke WR, Vatish M, Dias-Neto E *et al* (2022) In sickness and in health: The functional role of extracellular vesicles in physiology and pathology in vivo: Part II: Pathology: Part II: Pathology. *J Extracell Vesicles* 11: e12190.

You Y, Borgmann K, Edara VV, Stacy S, Ghorpade A, Ikezu T (2020) Activated human astrocyte-derived extracellular vesicles modulate neuronal uptake, differentiation and firing. *J Extracell Vesicles* 9: 1706801.

Zhang Y, Chopp M, Liu XS, Katakowski M, Wang X, Tian X, Wu D, Zhang ZG (2017) Exosomes Derived from Mesenchymal Stromal Cells Promote Axonal Growth of Cortical Neurons. *Mol Neurobiol* 54: 2659-2673.

Zhang Y, Liu Y, Liu H, Tang WH (2019) Exosomes: biogenesis, biologic function and clinical potential. *Cell Biosci* 9: 19.

Zhao Y, Liang Y, Xu Z, Liu J, Liu X, Ma J, Sun C, Yang Y (2022) Exosomal miR-673-5p from fibroblasts promotes Schwann cell-mediated peripheral neuron myelination by targeting the TSC2/mTORC1/SREBP2 axis. *J Biol Chem* 298: 101718.

Zhao Y, Liu J, Liu S, Yang P, Liang Y, Ma J, Mao S, Sun C, Yang Y (2023) Fibroblast exosomal TFAP2C induced by chitosan oligosaccharides promotes peripheral axon regeneration via the miR-132-5p/CAMKK1 axis. *Bioact Mater* 26: 249-263.

Zou Y (2020) Breaking symmetry - cell polarity signaling pathways in growth cone guidance and synapse formation. *Curr Opin Neurobiol* 63: 77-86.

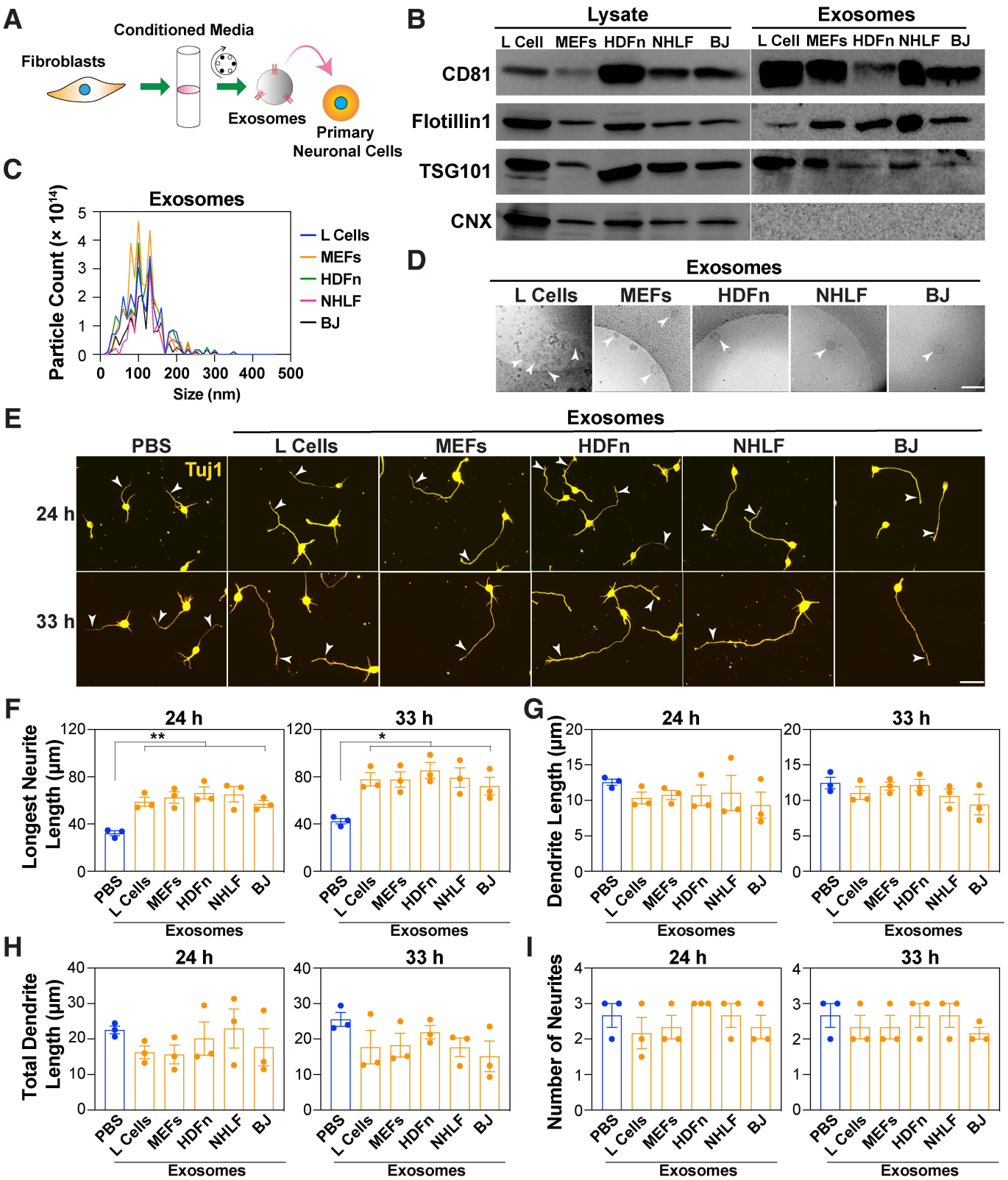
A
Conditioned Media
Fibroblasts
Exosomes
Primary Neuronal Cells
B
Lysate
Exosomes
L Cell MEFs HDFn NHLF BJ
L Cell MEFs HDFn NHLF BJ
CD81
Flotillin1
TSG101
CNX
C
Exosomes
Particle Count (× 10^14)
Size (nm)
L Cells
MEFs
HDFn
NHLF
BJ
D
Exosomes
L Cells MEFs HDFn NHLF BJ
E
Exosomes
PBS L Cells MEFs HDFn NHLF BJ
Tuj1
24 h
33 h
F
24 h
33 h
Longest Neurite Length (µm)
PBS L Cells MEFs HDFn NHLF BJ
Exosomes
G
24 h
33 h
Dendrite Length (µm)
H
24 h
33 h
Total Dendrite Length (µm)
I
24 h
33 h
Number of Neurites

Figure 1

Figure 1. Exosomes promote the growth of the prospective axon. (A) A schematic of the experimental set up. Mouse cortical neurons (E15.5-16.5) are treated with exosomes isolated from fibroblast-conditioned media (CM) using differential centrifugation. (**B)** Representative immunoblotting of cell lysates and exosome pellets (100,000 x g) from the indicated fibroblast cell lines for exosome markers CD81, Flotillin1 and TSG101 and the ER protein, calnexin (CNX). (**C)** Nanoparticle tracking analysis (NTA) of differential centrifugation pellets. A representative plot indicating the particle size distribution from 3 independent purifications is shown. (**D)** Representative transmission electron microscopy (TEM) images of exosome-containing pellets. Arrowheads indicate round vesicles. Scale bar, 200 nm. (**E-I)** Cortical neurons were treated with exosomes (5 µg/mL) purified from the indicated fibroblast cell lines, 4 h after plating. Neurons were fixed at 24 and 33 h, and neuronal morphology was examined after staining for Tuj1. **(E)** Representative images are shown. Arrowheads mark the longest neurite. Scale bar, 40 µm. **(F-I)** The length of the longest neurite (prospective axon; **F**), individual neurite/dendrite lengths **(G)**, total dendrite length (longest neurite excluded; **H**) and total number of neurites **(I)** were quantified from a minimum of 90 neurons from 3 independent experiments and is plotted as the average of the median ± SEM. Each dot represents the median length of 30 neurons from one of the three independent experiments. Statistical significance: *$p<0.05$, **$p<0.01$using one-way ANOVA with Dunnetts post-test.

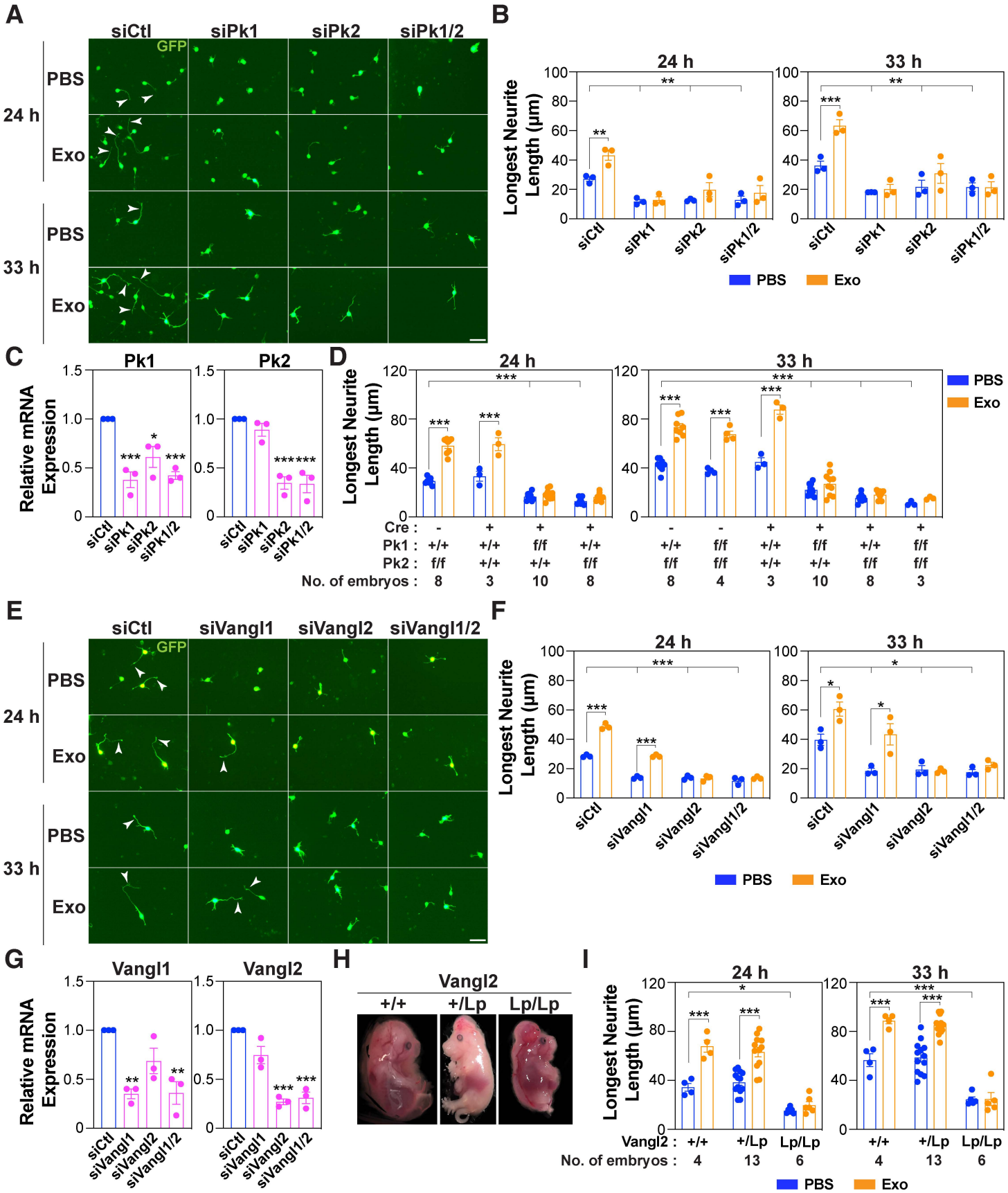
A
siCtl
siPk1
siPk2
siPk1/2
GFP
24 h
33 h
PBS
Exo
B
24 h
33 h
Longest Neurite Length (μm)
PBS
Exo
C
Pk1
Pk2
Relative mRNA Expression
D
24 h
33 h
Cre :
Pk1 :
Pk2 :
No. of embryos :
E
siVangl1
siVangl2
siVangl1/2
F
G
Vangl1
Vangl2
H
+/+
+/Lp
Lp/Lp
I
Vangl2 :
No. of embryos :

Figure 2

Figure 2. The PCP components, Pk1/2 and Vangl2, are required for exosome-induced growth of the longest neurite. (A-C, E-G) Pk1/2 and Vangl2 promote exosome-induced neurite outgrowth. Dissociated E15.5-16.5 mouse cortical neurons were electroporated with siRNA against Pk1 (siPk1) and Pk2 (siPk2) (**A-C**), or Vangl1 (siVangl1) and Vangl2 (siVangl2) (**E-G**) individually or in combination or with siControl (siCtl) along with a GFP-expressing plasmid and were treated with exosomes (5 µg/mL) from L cells, 4 h after plating. Neurons were fixed at 24 and 33 h, and neuronal morphology was examined in GFP-positive neurons. (**A, E**) Representative images are shown. Arrowheads mark the longest neurite. Scale bar, 40 µm. (**B, F**) The length of the longest neurites was quantified. (**C, G)** Knockdown efficiency for Pk1/Pk2 (**C**) and Vangl1/2 (**G**) was determined in GFP-positive neurons isolated by FACS. Relative mRNA expression was determined by qPCR. (**D, I)** Pk1/2 and Vangl2 promote exosome-induced neurite outgrowth in mutant mouse models. Cortical neurons (E15.5-16.5) were isolated from Pk1 and Pk2 conditional knockout mice obtained by crossing Pk floxed mice with a Nestin-Cre line **(D)** or Vangl2 mutant littermates obtained by crossing of heterozygous loop-tail mutants ($Vangl2^{+/Lp}$) **(I).** Neurons were treated with exosomes from L cells, 4 h after plating, fixed at 24 and 33 h and morphology examined in Tuj1 stained neurons. The length of the longest neurite was quantified from 40 neurons per embryo, and total number of embryos analyzed are indicated below the genotypes. **(H)** Loop-tail embryos exhibit an open neural tube. Representative images are shown from a minimum 4 independent experiments.

For all plots, data is presented as the mean ± SEM from a minimum 3 independent experiments. In neuronal morphology experiments, each dot represents the median length of a minimum of 30 neurons from one of the three independent experiments **(B, D, F, I**). Statistical significance: *$p<0.05$, **$p<0.01$, ***$p<0.001$ using one-way ANOVA with Dunnetts post-test **(C, G)**, or two-way ANOVA with Tukey's post-test **(B, D, F, I)**.

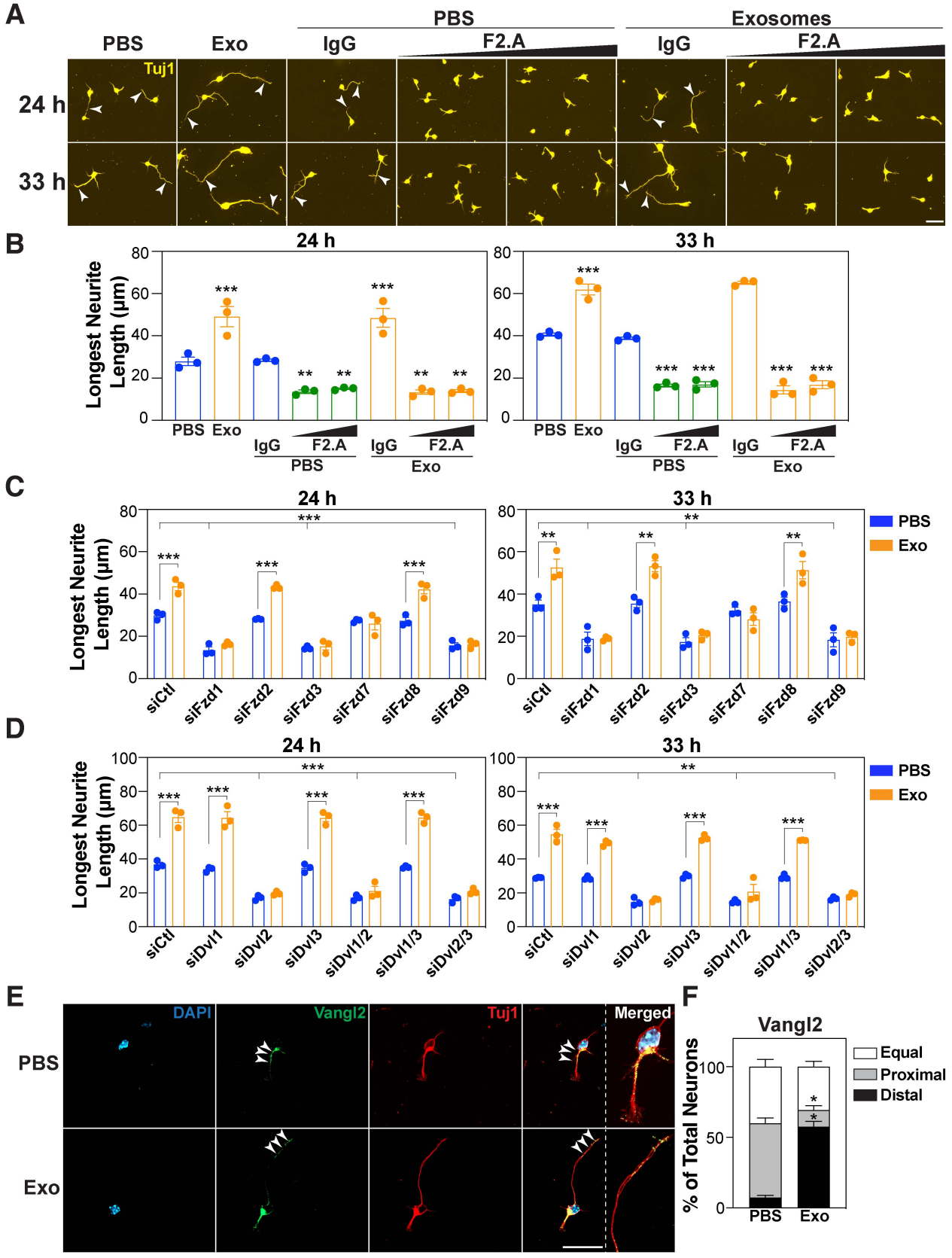
A
PBS
Exo
PBS
IgG
F2.A
Exosomes
IgG
F2.A
Tuj1
24 h
33 h
B
24 h
33 h
Longest Neurite Length (μm)
PBS Exo
IgG F2.A
PBS
IgG F2.A
Exo
C
24 h
33 h
Longest Neurite Length (μm)
PBS
Exo
siCtl
siFzd1
siFzd2
siFzd3
siFzd7
siFzd8
siFzd9
D
24 h
33 h
Longest Neurite Length (μm)
PBS
Exo
siCtl
siDvl1
siDvl2
siDvl3
siDvl1/2
siDvl1/3
siDvl2/3
E
DAPI
Vangl2
Tuj1
Merged
PBS
Exo
F
Vangl2
% of Total Neurons
Equal
Proximal
Distal
PBS
Exo

Figure 3

Figure 3. Fzds and Dvls are required for exosome-induced growth of the longest neurite. **(A-D)** Dissociated E15.5-16.5 mouse cortical neurons were treated with exosomes (5 µg/mL) from L cells, 4 h after plating. **(A-B)** Neurons were co-treated with IgG or a Fzd blocking antibody, F2.A (at 50 nM and 100 nM) along with exosomes. **(C-D)** Neurons were electroporated with siRNA against Fzds (siFzds) **(C)**, or Dvls (siDvl) **(D)** or siControl in combination with a GFP-expressing plasmid prior to the addition of exosomes. Neurons were fixed at 24 and 33 h, and neuronal morphology was examined in Tuj1 stained **(A, B)** or GFP-positive neurons **(C, D)** with representative images shown. Arrowheads mark the longest neurite. Scale bar, 40 µm. **(B-D)** The length of the longest neurite was quantified. **E)** Exosomes promote localization of Vangl2 to the distal axon. Cortical neurons were treated with exosomes from L cells, 4 h after plating and fixed after 24 h. Representative confocal images of neurons stained with DAPI (blue), Vangl2 (green) and Tuj1 (red) are shown. Arrowheads mark the Vangl2 localization. (**F)** The percent of neurons displaying the indicated Vangl2 distribution is quantified from 30 neurons from 3 independent experiments.

For all plots, data is presented as mean ± SEM from 3 independent experiments (**B, C, D, F)**. In neuronal morphology experiments, each dot represents the median length of minimum 30 neurons from one of the three independent experiments **(B, C, D)**. Statistical significance: *$p<0.05$, **$p<0.01$, ***$p<0.001$ using either one-way ANOVA with Dunnetts post-test **(B)**, or two-way ANOVA with Tukey's post-test **(C, D, F)**.

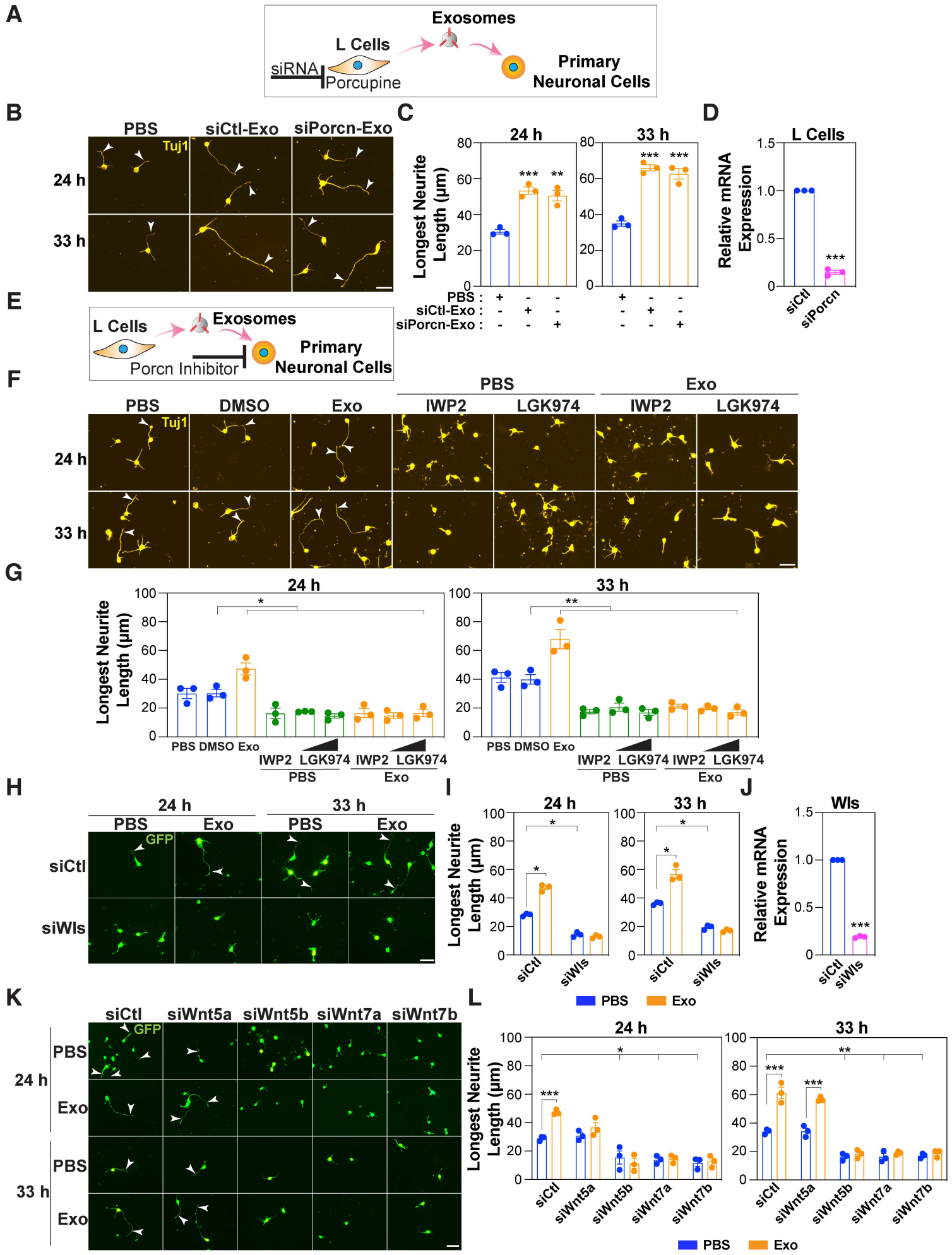
A
Exosomes
L Cells
siRNA
Porcupine
Primary Neuronal Cells
B
PBS
siCtl-Exo
siPorcn-Exo
Tuj1
24 h
33 h
C
24 h
33 h
Longest Neurite Length (μm)
PBS :
siCtl-Exo :
siPorcn-Exo :
D
L Cells
Relative mRNA Expression
siCtl
siPorcn
E
L Cells
Exosomes
Porcn Inhibitor
Primary Neuronal Cells
F
PBS
DMSO
Exo
IWP2
LGK974
G
PBS DMSO Exo
IWP2 LGK974 IWP2 LGK974
H
GFP
siCtl
siWls
I
J
Wls
K
siWnt5a
siWnt5b
siWnt7a
siWnt7b
L
PBS
Exo

Figure 4

Figure 4. Autocrine Wnt Signaling mediates exosome-induced growth of the longest neurite. (A, E) Schematics, illustrating the experimental set up. **(A-G)** Dissociated E15.5-16.5 mouse cortical neurons are treated with exosomes isolated from L cells transfected with siCtl or siPorcupine **(A-D)** or with exosomes isolated from regular L cells. Neurons were treated with PBS as control and with porcupine (Porcn) inhibitors, IWP2 (10 μM) or LGK974 (1 and 5 μM) **(E-G)**, 4 h after plating and were co-incubated with exosomes. (**H-L)** Cortical neurons were electroporated with siRNAs against Wls (siWls) **(H, I)** or Wnts (siWnts) **(K, L)** or siControl (siCtl) along with a GFP-expressing plasmid and then treated with exosomes (5 μg/mL) from L cells, 4 h after plating. Neurons were fixed at 24 and 33 h, and neuronal morphology was examined in Tuj1 stained neurons **(B, C, F, G)** or GFP-positive neurons for siRNA experiments **(H, I, K, L)**. Representative images **(B, F, H, K)** and quantifications of the longest neurite **(C, G, I, L)** are shown. (**D, J)** Knockdown efficiency for porcupine **(D)** and Wls **(J)** was determined in L cells and GFP-positive neurons isolated by FACS, respectively. Relative mRNA expression was determined by qPCR.

For all plots, data is presented as the mean ± SEM from 3 independent experiments **(C, D, G, I, J, L)**. In neuronal morphology experiments, each dot represents the median length of minimum 30 neurons from one of the three independent experiments **(C, G, I, L)**. Statistical significance: *$p<0.05$, **$p<0.01$, ***$p<0.001$ using unpaired t-test **(D, J)**, one-way ANOVA with Dunnetts post-test **(C, G)**, or two-way ANOVA with Tukey's post-test **(I, L)**.

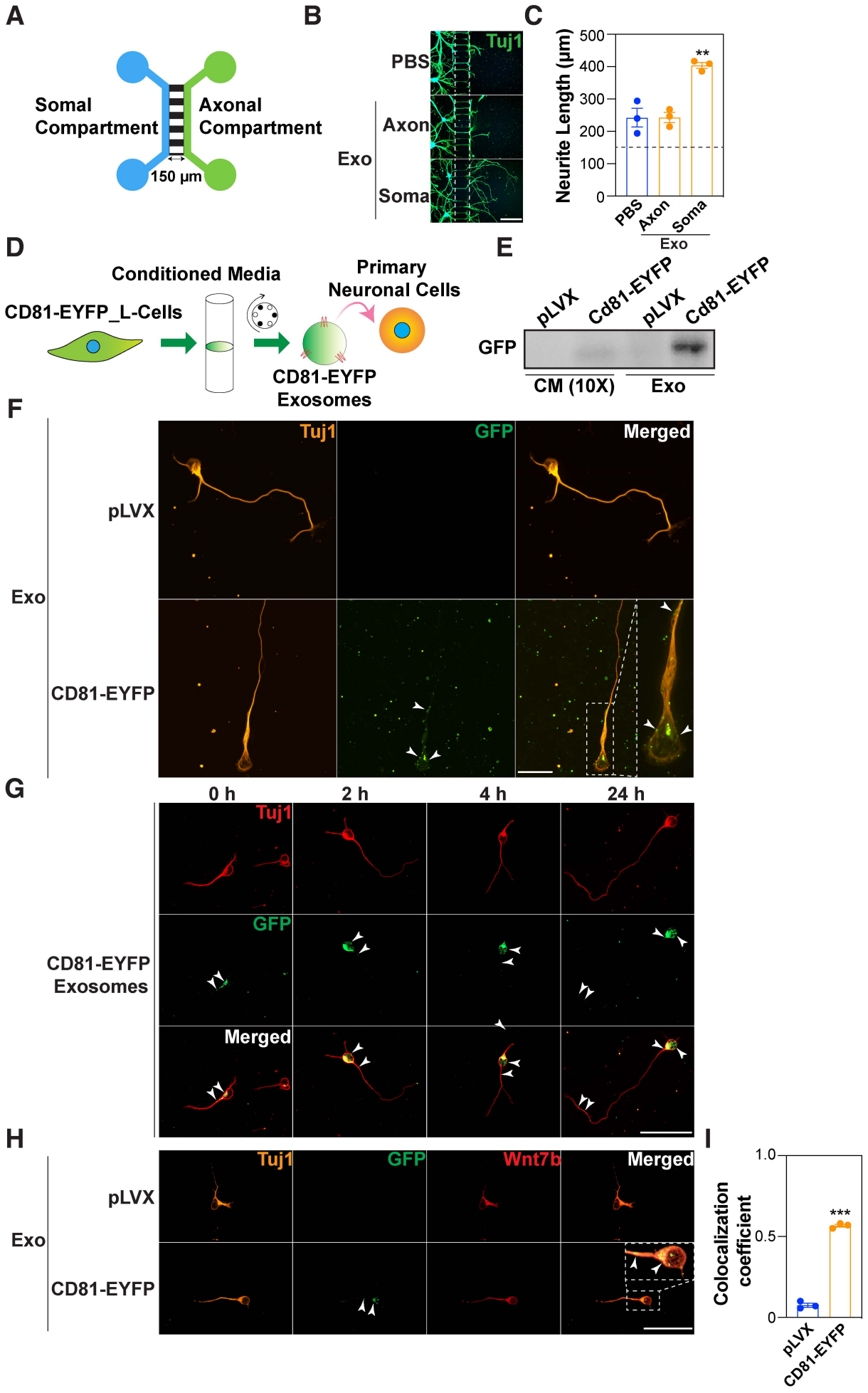
A
Somal Compartment
Axonal Compartment
150 µm
B
Tuj1
PBS
Exo
Axon
Soma
C
Neurite Length (µm)
500
400
300
200
100
0
**
PBS
Axon
Soma
Exo
D
Conditioned Media
CD81-EYFP_L-Cells
Primary Neuronal Cells
CD81-EYFP Exosomes
E
pLVX
Cd81-EYFP
pLVX
Cd81-EYFP
GFP
CM (10X)
Exo
F
Tuj1
GFP
Merged
pLVX
Exo
CD81-EYFP
G
0 h
2 h
4 h
24 h
Tuj1
GFP
Merged
CD81-EYFP Exosomes
H
Tuj1
GFP
Wnt7b
Merged
pLVX
Exo
CD81-EYFP
I
Colocalization coefficient
1.0
0.5
0
***
pLVX
CD81-EYFP

Figure 5

Figure 5. Exosomes promote neurite elongation and co-localize with Wnt7b. (A-C) Exosomes promote neurite elongation. **(A)** A schematic illustration of the two compartment Xona microfluidic device. The somal compartment is connected to axonal compartment through a 150 μm microgroove. **(B)** Cortical neurons (E15.5-16.5) were seeded in the somal compartment and cultured for 5 days prior to the addition of the L cell-derived exosomes in either the somal or axonal compartment. Neurons were fixed 24 h later and neuronal morphology was examined in Tuj1 stained neurons. Representative images are shown. Scale bar, 200 μm. **(C)** The length of the neurites growing in the microgroove and emerging in the axonal compartment was quantified for a minimum of 90 neurites. A dotted line marks both ends of the microgroove (150 μm). **(D-I)** Exoxomes can be internalized by neurons and associate with Wnts. Cortical neurons were treated with 10X conditioned-media from L cells stably expressing CD81-EYFP, 4 h after plating for 29 h **(F)** or 24 h after plating for 30 min **(G, H)**. In panel **G**, after 30 min of treatment, neurons were washed and subsequently treated with regular complete media for 0, 2, 4 and 24 h. Representative images of neurons immunostained with GFP and Tuj1 **(F, G)** or GFP, Tuj1 and Wnt7b **(H)** are shown. Scale bar, 20 μm **(F)** or 40 μm **(G, H)**. **(E)** Exosome characterization. The concentrated CM (10X) and exosome pellet (Exo) from L cells were immunoblotted with anti-GFP antibody. **(I)** Pearson's colocalization coefficient for **(H)**. Neurons were identified using Tuj1 as a reference channel and the colocalization coefficient was quantified using Nikon NIS-Elements software.

Images **(F, G, H)** and the quantification **(F)** are representative of 30 neurons from 3 independent experiments. Statistical significance: **$p<0.01$, ***$p<0.001$ using unpaired t-test **(I)** or one-way ANOVA with Dunnetts post-test **(C)**.

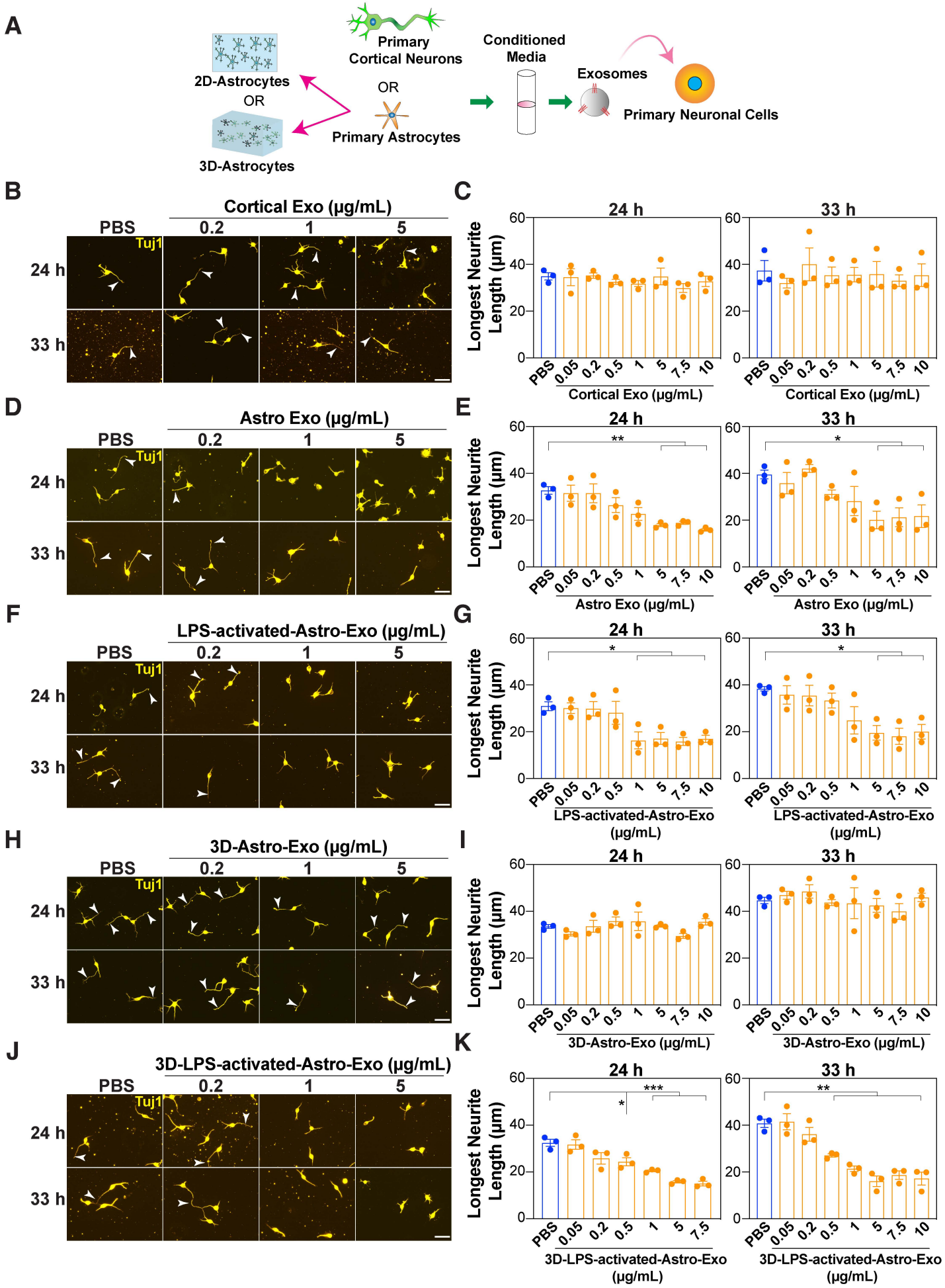
A
2D-Astrocytes
OR
3D-Astrocytes
Primary Cortical Neurons
OR
Primary Astrocytes
Conditioned Media
Exosomes
Primary Neuronal Cells
B
Cortical Exo (μg/mL)
PBS
0.2
1
5
Tuj1
24 h
33 h
C
24 h
33 h
Longest Neurite Length (μm)
PBS
0.05
0.2
0.5
1
5
7.5
10
Cortical Exo (μg/mL)
D
Astro Exo (μg/mL)
E
**
*
Astro Exo (μg/mL)
F
LPS-activated-Astro-Exo (μg/mL)
G
LPS-activated-Astro-Exo (μg/mL)
H
3D-Astro-Exo (μg/mL)
I
3D-Astro-Exo (μg/mL)
J
3D-LPS-activated-Astro-Exo (μg/mL)
K
***
3D-LPS-activated-Astro-Exo (μg/mL)

Figure 6

Figure 6. Exosomes from neurons and astrocytes do not promote growth of the longest neurite. **(A)** A schematic illustration of the experimental set up. Dissociated E15.5-16.5 cortical neurons were treated with exosomes purified from primary cortical neurons or primary astrocytes. **(B-K)** Cortical neurons were treated with various concentrations (0.05-10 μg/mL) of exosomes purified from cortical neurons **(B, C),** astrocytes **(D, E),** LPS-activated astrocytes **(F, G),** 3D-astrocytes grown in collagen gel **(H, I)** and LPS-activated 3D-astrocytes **(J, K)**, 4 h after plating. Neurons were fixed at 24 and 33 h, and neuronal morphology was examined in Tuj1 stained neurons. Representative images (**B, D, F, H, J**) and quantifications (**C, E, G, I, K**) are shown. Arrowheads mark the longest neurite. Scale bar, 40 μm.

Values are plotted as the average of the median ± SEM from 3 independent experiments. Each dot represents the median length of minimum 40 neurons from one of the three independent experiments. Statistical significance: *$p<0.05$, **$p<0.01$, ***$p<0.001$ using one-way ANOVA with Dunnetts post-test.

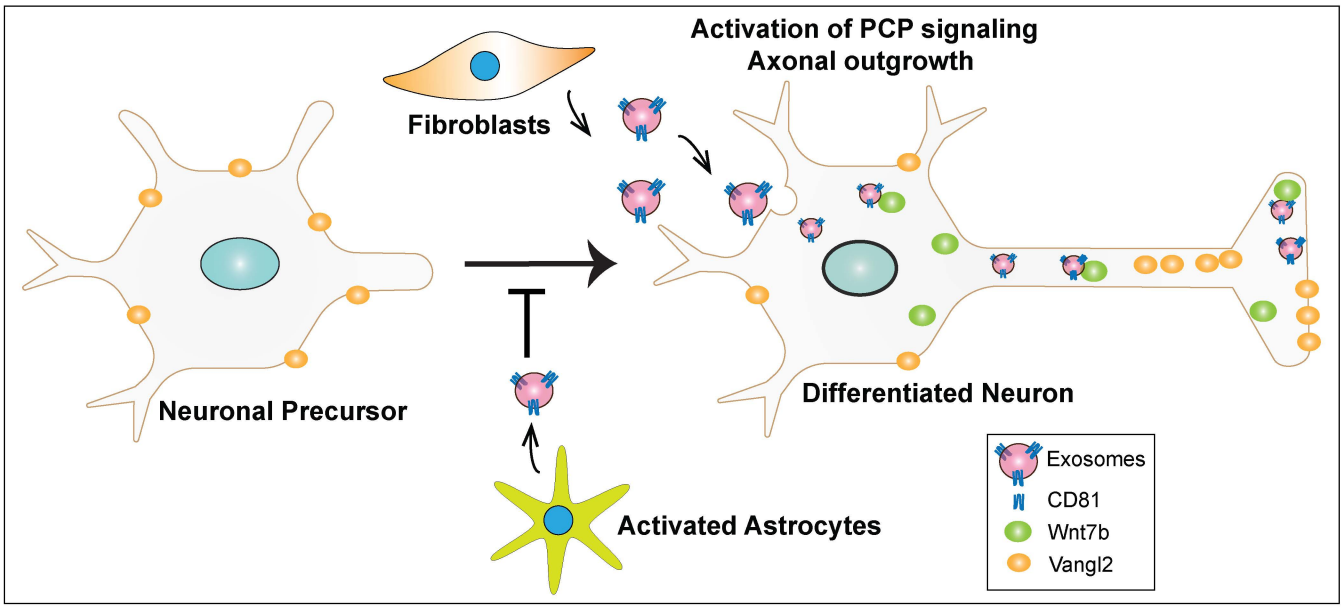

Figure 7. A model, depicting the role of exosomes in promoting axon outgrowth and polarized neuronal morphology through Wnt-PCP signaling. Exosomes secreted by L cells mobilize autocrine Wnt-PCP signaling in neurons to promote axon outgrowth that results in the acquisition of a polarized neuronal morphology. Exosomes induce a shift in Vangl2 localization towards distal axon. Exosomes can be internalized by neurons and can co-localize with Wnt7b to promote the growth of the prospective axon. In contrast to fibroblast derived exosomes, those isolated from activated astrocytes inhibit neurite outgrowth.

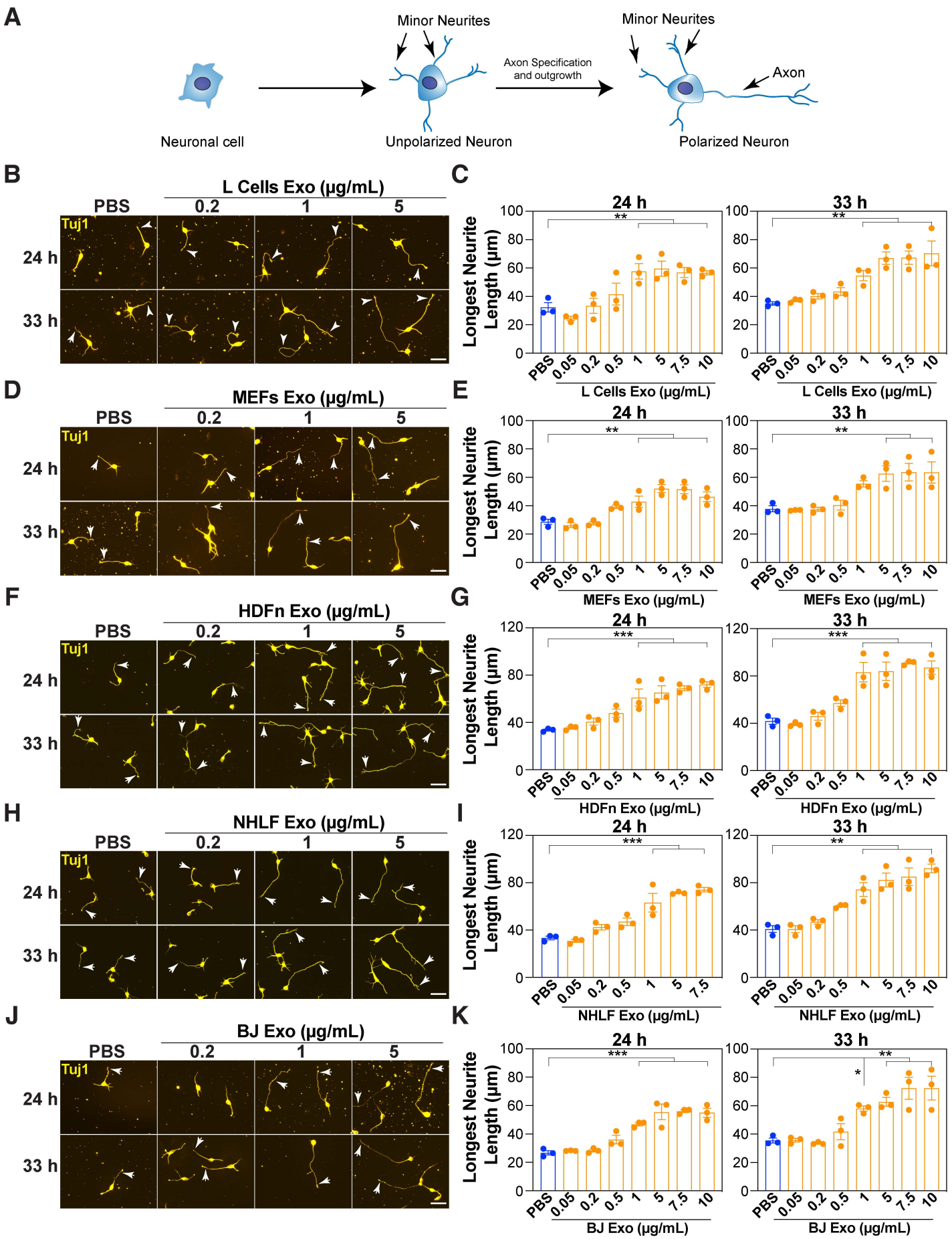
A
Minor Neurites
Minor Neurites
Axon Specification and outgrowth
Axon
Neuronal cell
Unpolarized Neuron
Polarized Neuron
B
L Cells Exo (μg/mL)
PBS
0.2
1
5
Tuj1
24 h
33 h
C
24 h
33 h
Longest Neurite Length (μm)
PBS
0.05
0.2
0.5
1
5
7.5
10
L Cells Exo (μg/mL)
D
MEFs Exo (μg/mL)
E
MEFs Exo (μg/mL)
F
HDFn Exo (μg/mL)
G
HDFn Exo (μg/mL)
H
NHLF Exo (μg/mL)
I
NHLF Exo (μg/mL)
J
BJ Exo (μg/mL)
K
BJ Exo (μg/mL)

Figure S1

Figure S1. Exosomes promote the growth of the longest neurite in a concentration-dependent manner. Related to Fig. 1. (A) A schematic of the morphological changes in neurons cultured *in vitro*. **(B-K)** Dissociated E15.5-16.5 mouse cortical neurons were treated with various concentrations (0.05-10 μg/mL) of exosomes purified from the indicated fibroblast cell lines including L cells **(B, C)**, MEFs **(D, E)**, HDFn **(F, G)**, NHLF **(H, I)** and BJ **(J, K),** 4 h after plating. Neurons were fixed at 24 and 33 h, and neuronal morphology was examined in Tuj1 stained neurons. Representative images **(B, D, F, H, J)** and quantifications **(C, E, G, I, K)** are shown. Arrowheads mark the longest neurite. Scale bar, 40 μm.

Values are plotted as the average of the median ± SEM from 3 independent experiments. Each dot represents the median length of at least 30 neurons from one of three independent experiments. Statistical significance: *$p<0.05$, **$p<0.01$, ***$p<0.001$ using one-way ANOVA with Dunnetts post-test.

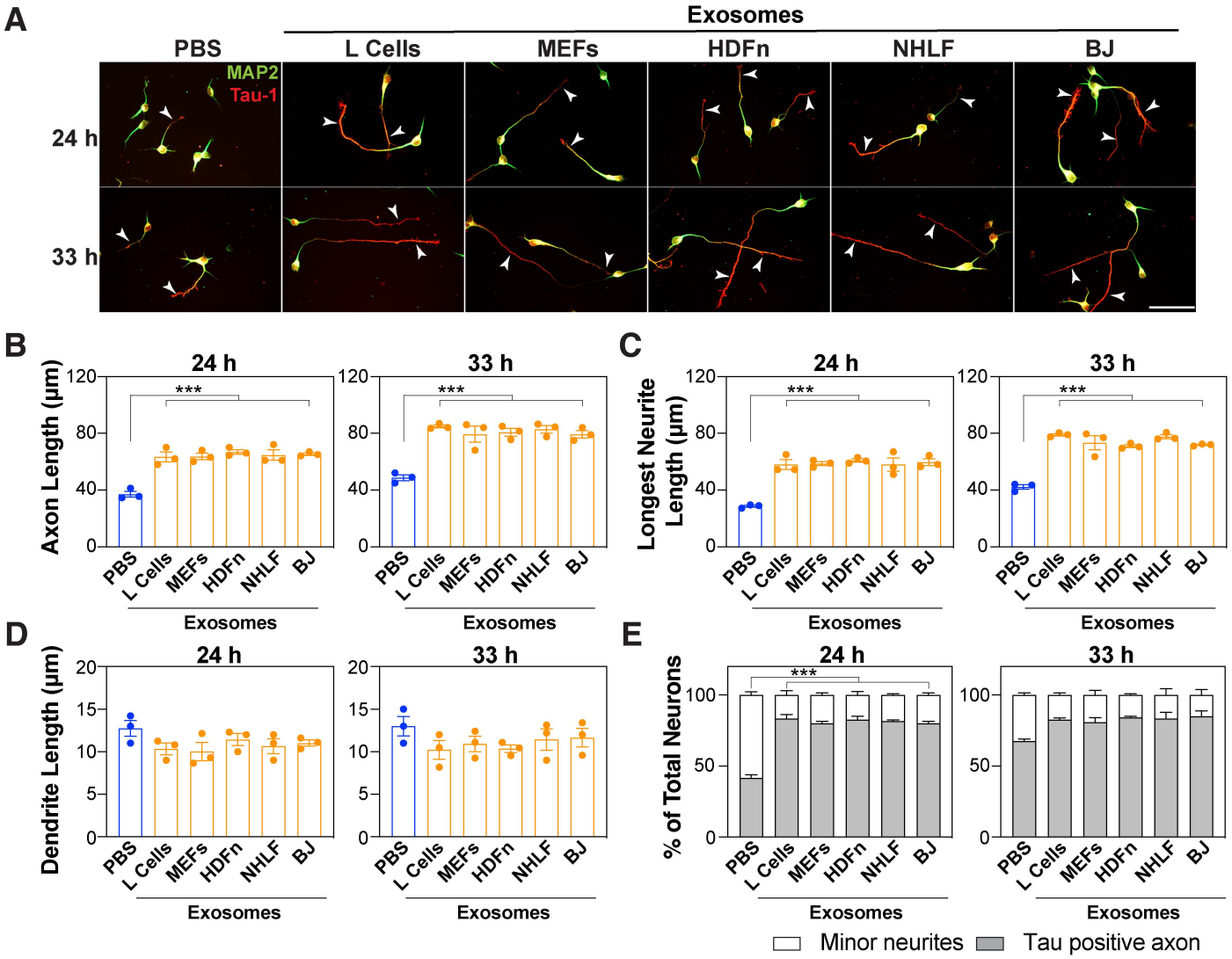

Figure S2. Exosomes promote axon outgrowth and polarized neuronal morphology. Related to Fig. 1. (**A**) Dissociated E15.5-16.5 mouse cortical neurons were treated with exosomes purified from the indicated fibroblast cell lines, 4 h after plating. Neurons were fixed at 24 and 33 h, and neuronal morphology was examined in neurons immunostained for MAP2 (dendrites, green) and Tau-1 (axons, red). Representative images are shown. Arrowheads mark Tau-1 positive axons. Scale bar, 50 µm. (**B-E**) The length of the Tau-1 positive axons **(B)**, longest neurite (independent of Tau-1+ staining, **C**) and individual dendrite length (MAP2 positive, **D**) is quantified. (**E**) Percent of neurons containing only minor neurites (MAP2 positive, but negative for Tau-1) or a single Tau-1-positive axon, is plotted. Values are plotted as an average of the median ± SEM from 3 independent experiments. Each dot represents the median length of at least 15 (for 24 h in panel **B**) or 30 (for all others) neurons from one of the three independent experiments. In panel **B**, for the 24 h control group (PBS treated), median was determined from 15 neurons per experiment due to greater percentage of neurons lacking a Tau-1 positive axon. Statistical significance: ***$p<0.001$ using one-way ANOVA with Dunnetts post-test **(B, C, D)**, or two-way ANOVA with Tukey's post-test **(E)**.

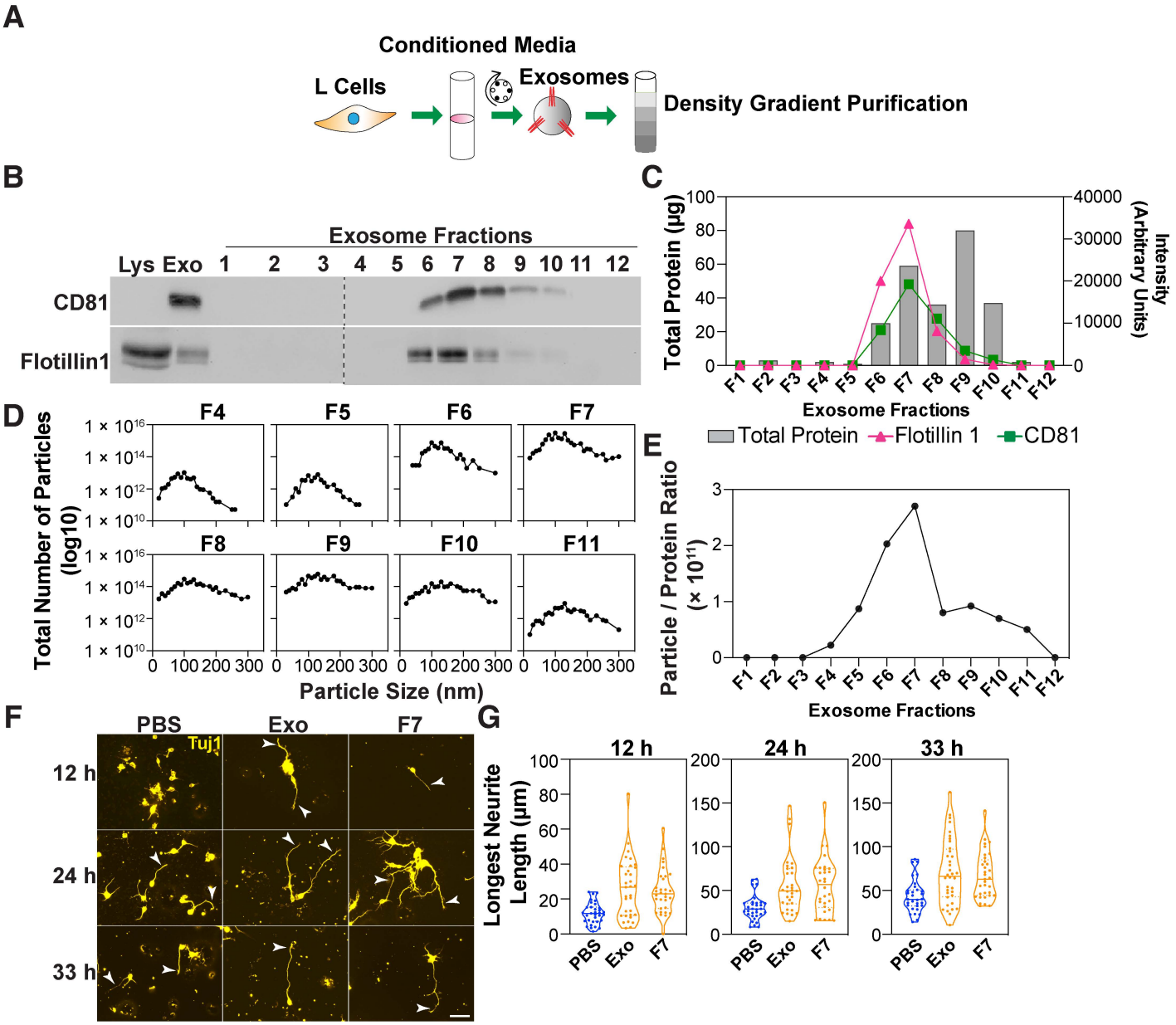

Figure S3. Exosomes isolated using a discontinuous density gradient promote the growth of the longest neurite. Related to Fig. 1. (A) A schematic of the experimental set up. Exosome pellets (100,000 x g) purified from the conditioned media (CM) of L cells using differential centrifugation were subjected to iodixanol discontinuous density gradient purification. **(B)** Twelve fractions were collected starting from the top of the discontinuous gradient and were analyzed by immunoblotting for the indicated exosomal markers. **(C)** Intensity of the bands of exosomal markers from **(B)** is plotted against the protein concentration. **(D)** Particle size distribution was determined using NTA. **(E)** Fraction 7 (F7) has the highest particle number/protein ratio. **(F)** F7 fraction promotes the growth of the longest neurite. Dissociated E15.5-16.5 cortical neurons were treated with the resuspended exosome pellet (Exo) and the F7 fraction (both at 2×10^8 particles/mL), 4 h after plating. Neuronal morphology was examined in Tuj1 stained neurons at 12, 24 and 33 h. Representative images are shown. Arrowheads mark the longest neurite. Scale bar, 40 µm. **(G)** A representative violin plot shows the length of the longest neurite with median marked from minimum 30 neurons from 2 independent experiments.

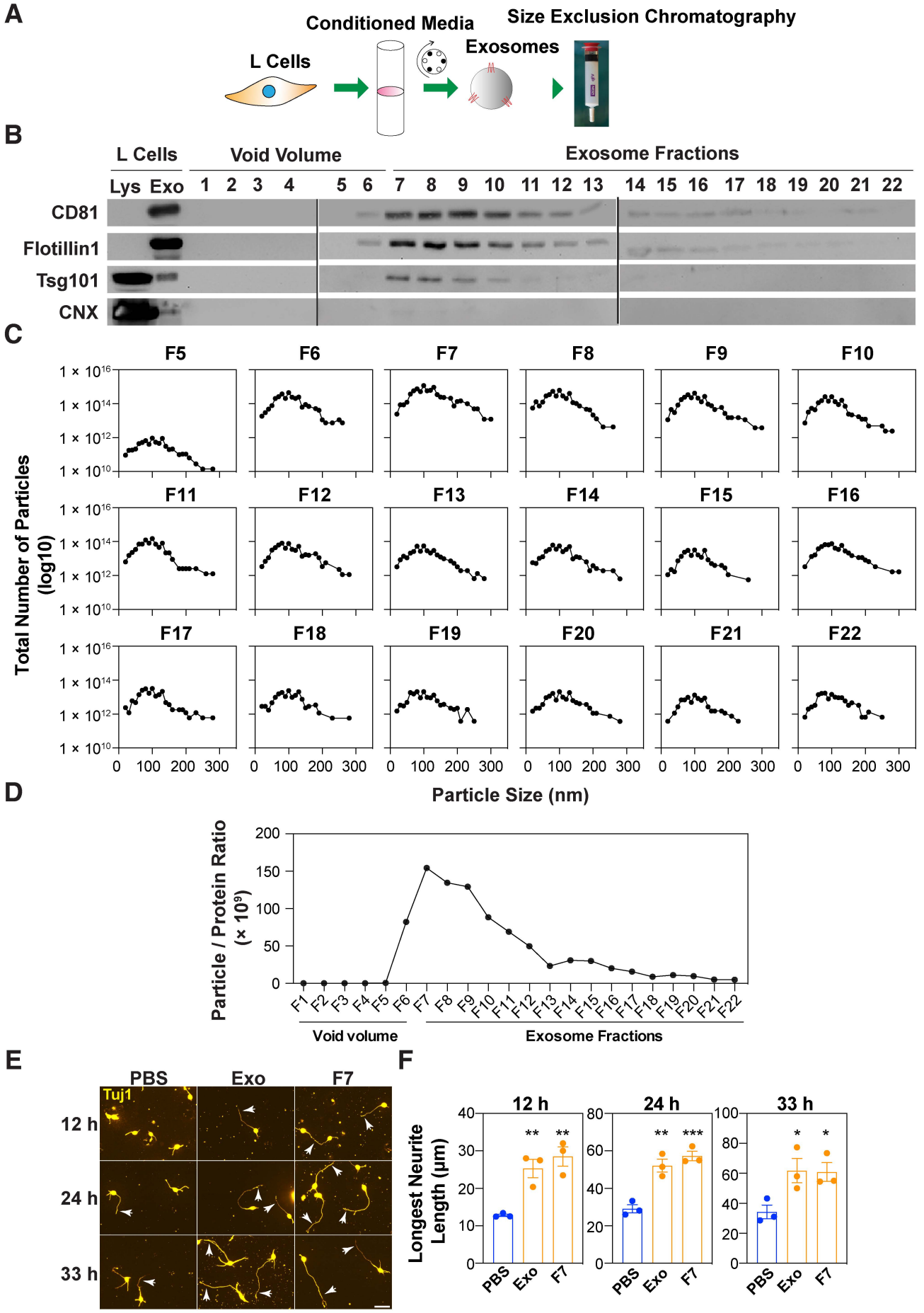
A
Conditioned Media
Size Exclusion Chromatography
L Cells
Exosomes
B
L Cells
Void Volume
Exosome Fractions
Lys Exo 1 2 3 4 5 6 7 8 9 10 11 12 13 14 15 16 17 18 19 20 21 22
CD81
Flotillin1
Tsg101
CNX
C
F5 F6 F7 F8 F9 F10
F11 F12 F13 F14 F15 F16
F17 F18 F19 F20 F21 F22
Total Number of Particles (log10)
1 × 10^16
1 × 10^14
1 × 10^12
1 × 10^10
0 100 200 300
Particle Size (nm)
D
Particle / Protein Ratio (× 10^9)
200
150
100
50
0
F1 F2 F3 F4 F5 F6 F7 F8 F9 F10 F11 F12 F13 F14 F15 F16 F17 F18 F19 F20 F21 F22
Void volume
Exosome Fractions
E
PBS
Exo
F7
Tuj1
12 h
24 h
33 h
F
12 h
24 h
33 h
Longest Neurite Length (μm)
PBS
Exo
F7
**
***
*

Figure S4

Figure S4. Exosomes isolated using size exclusion chromatography promote the growth of the longest neurite. Related to Fig. 1. (A) A schematic illustration of experimental set up. Exosomes purified from the CM of L cells were subjected to size exclusion chromatography. **(B)** A total of 22 fractions were collected and subjected to immunoblotting for exosomal markers. **(C)** Particle size was measured using NTA. **(D)** Fraction 7 (F7) has the highest particle number/protein ratio. **(E)** F7 fraction promotes the growth of the longest neurite. Dissociated E15.5-16.5 cortical neurons were treated with resuspended 100,000 x g pellet (Exo, 5 μg/mL) and F7 fraction (5 μg/mL), 4 h after plating. Neuronal morphology was examined in Tuj1 stained neurons at various time points: 12, 24 and 33 h. Representative images are shown. Arrowheads mark the longest neurite. Scale bar, 40 μm **(F)** The length of the longest neurite was quantified and plotted as the average of the median ± SEM from 3 independent experiments. Each dot represents the median length of a minimum 30 neurons from one of three independent experiments. Statistical significance: *$p<0.05$, **$p<0.01$, ***$p<0.001$ using one-way ANOVA with Dunnetts post-test.

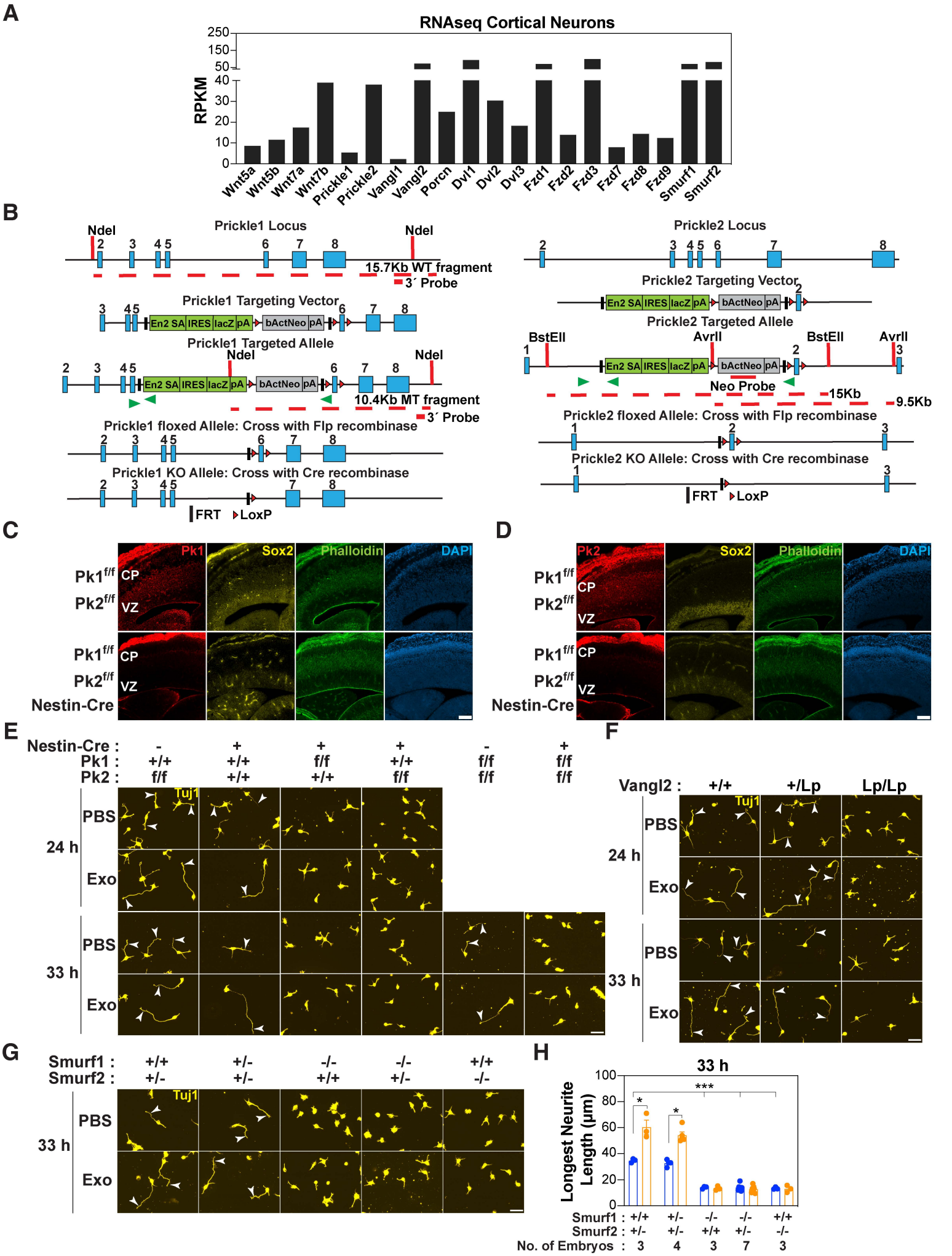
A
RNAseq Cortical Neurons
RPKM
250
150
50
40
30
20
10
0
Wnt5a
Wnt5b
Wnt7a
Wnt7b
Prickle1
Prickle2
Vangl1
Vangl2
Porcn
Dvl1
Dvl2
Dvl3
Fzd1
Fzd2
Fzd3
Fzd7
Fzd8
Fzd9
Smurf1
Smurf2
B
Prickle1 Locus
NdeI
15.7Kb WT fragment
3´ Probe
Prickle1 Targeting Vector
En2 SA
IRES
lacZ
pA
bActNeo
Prickle1 Targeted Allele
10.4Kb MT fragment
Prickle1 floxed Allele: Cross with Flp recombinase
Prickle1 KO Allele: Cross with Cre recombinase
FRT
LoxP
Prickle2 Locus
Prickle2 Targeting Vector
Prickle2 Targeted Allele
BstEII
AvrII
Neo Probe
15Kb
9.5Kb
Prickle2 floxed Allele: Cross with Flp recombinase
Prickle2 KO Allele: Cross with Cre recombinase
C
Pk1
Sox2
Phalloidin
DAPI
Pk1f/f
Pk2f/f
CP
VZ
Nestin-Cre
D
Pk2
E
Nestin-Cre :
Pk1 :
Pk2 :
Tuj1
PBS
Exo
24 h
33 h
F
Vangl2 :
+/+
+/Lp
Lp/Lp
G
Smurf1 :
Smurf2 :
H
33 h
Longest Neurite Length (µm)
No. of Embryos :

Figure S5

Figure S5. The PCP components, Pk1/2 and Vangl2, are required for exosome-induced growth of the longest neurite. Related to Fig. 2. (A) Expression of PCP genes and Wnts in cortical neurons. Total RNA was isolated from E15.5-16.5 cortical neurons after 33 h of *in vitro* culturing. An RNA sequence library was constructed, and high-quality reads were aligned to the *M. musculus* genome and expression of the indicated genes plotted. RPKM, Reads per kilobase of transcript per million mapped reads. (**B)** Schematic maps of the Pk1 and Pk2 wild type allele, targeting vector, targeted allele, floxed allele after crossing with Flp recombinase and knockout allele after crossing with Cre recombinase are shown. Green arrowheads indicate the position of PCR primers for genotyping. **(C, D)** Brain cryosections of E15.5 mouse embryo were stained with antibodies for Pk1 and Sox2 **(C)** or Pk2 and Sox2 **(D)** along with phalloidin. CP: cortical plate, VZ: ventricular zone. Scale bar, 100 μm. **(E-H)** Cortical neurons (E15.5-16.5) were isolated from Pk1 and Pk2 conditional knockout mice **(E)** or Vangl2 mutant littermates **(F)** or Smurf1 and Smurf2 knockout mice **(G, H)**, and treated with exosomes from L cells, 4 h after plating. Neurons were fixed at 24 and 33 h and stained with Tuj1. Representative images are shown. Arrowheads mark the longest neurite. Scale bar, 40 μm. **(H)** The length of the longest neurite was quantified from 30 neurons per embryo, and total number of embryos analyzed indicated below the genotypes. Statistical significance: *$p<0.05$, ***$p<0.001$ using two-way ANOVA with Tukey's post-test.

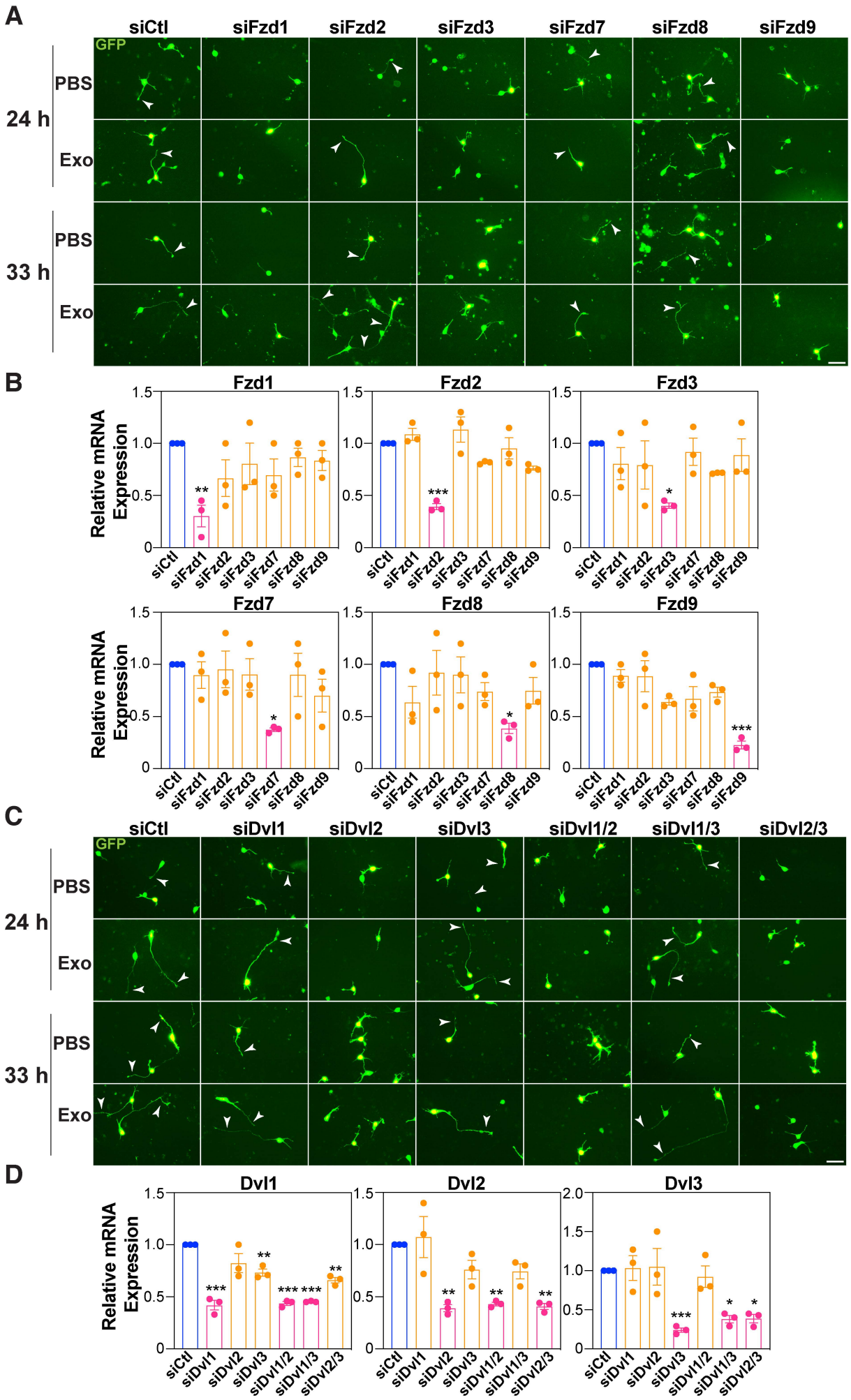
A
siCtl
siFzd1
siFzd2
siFzd3
siFzd7
siFzd8
siFzd9
GFP
24 h
PBS
Exo
33 h
PBS
Exo
B
Fzd1
Fzd2
Fzd3
Fzd7
Fzd8
Fzd9
Relative mRNA Expression
C
siCtl
siDvl1
siDvl2
siDvl3
siDvl1/2
siDvl1/3
siDvl2/3
GFP
24 h
PBS
Exo
33 h
PBS
Exo
D
Dvl1
Dvl2
Dvl3
Relative mRNA Expression

Figure S6

Figure S6. The PCP components, Fzds and Dvls, are required for exosome-induced growth of the longest neurite. Related to Fig. 3. (A, C) Representative images of dissociated E15.5-16.5 cortical neurons electroporated with siRNA against Fzds (siFzds) **(A)** or Dvls (siDvls) **(C)** or siControl (siCtl) along with a GFP-expressing plasmid and then treated with exosomes (5 μg/mL) from L cells, 4 h after plating. Arrowheads mark the longest neurite. Scale bar, 40 μm. **(B, D)** Knockdown efficiency for Fzds **(B)** and Dvls **(D)** was determined in GFP-positive neurons isolated by FACS. Relative mRNA expression was determined by qPCR and is plotted as the mean ± SEM from 3 independent experiments.

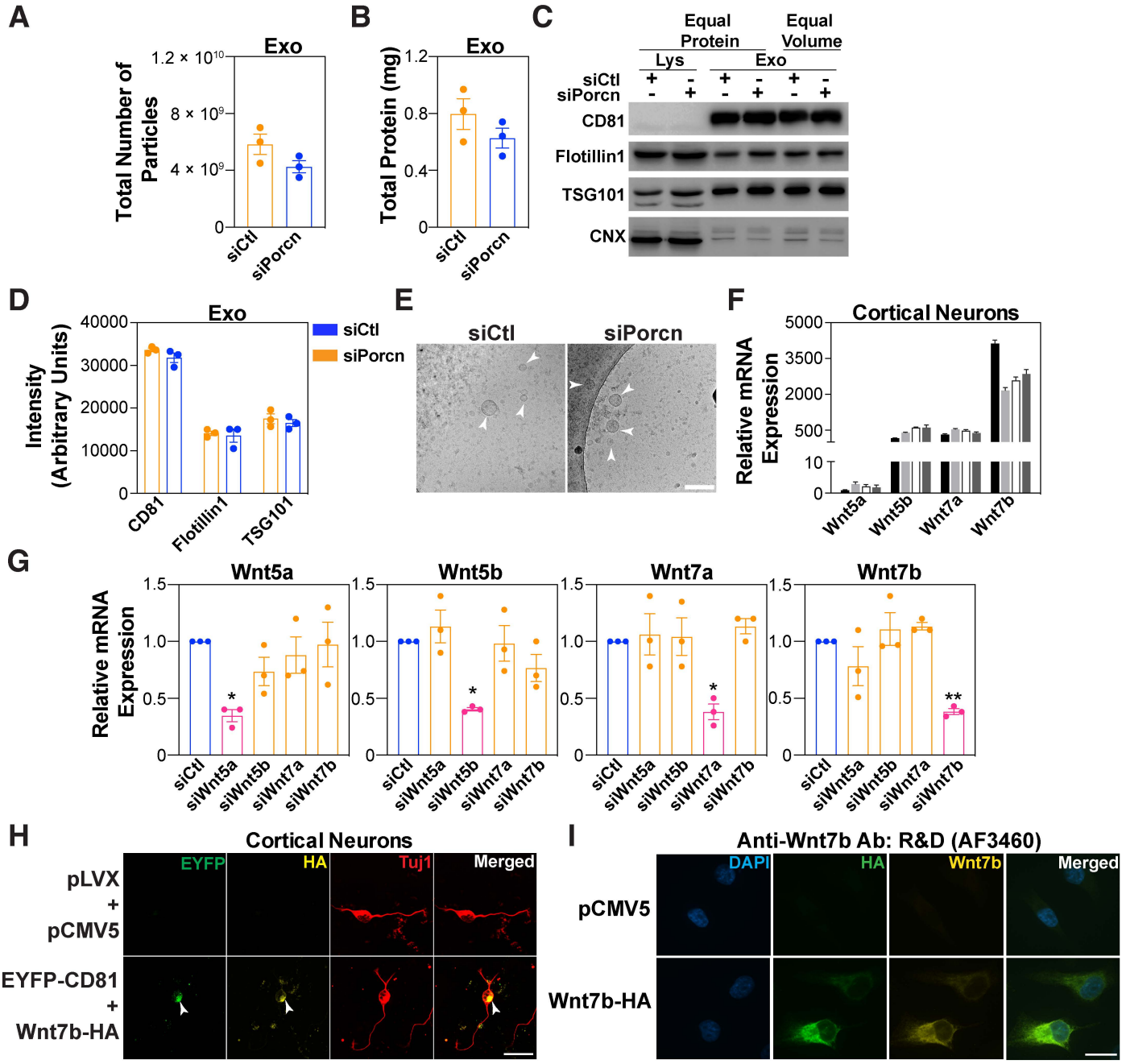
A
Exo
Total Number of Particles
1.2 × 10^10
8 × 10^9
4 × 10^9
0
siCtl
siPorcn
B
Exo
Total Protein (mg)
1.2
0.8
0.4
0
siCtl
siPorcn
C
Equal Protein
Equal Volume
Lys
Exo
siCtl
siPorcn
CD81
Flotillin1
TSG101
CNX
D
Exo
Intensity (Arbitrary Units)
40000
30000
20000
10000
0
siCtl
siPorcn
CD81
Flotillin1
TSG101
E
siCtl
siPorcn
F
Cortical Neurons
Relative mRNA Expression
5000
3500
2000
500
10
0
Wnt5a
Wnt5b
Wnt7a
Wnt7b
G
Wnt5a
Wnt5b
Wnt7a
Wnt7b
Relative mRNA Expression
1.5
1.0
0.5
0
siCtl
siWnt5a
siWnt5b
siWnt7a
siWnt7b
H
Cortical Neurons
EYFP
HA
Tuj1
Merged
pLVX + pCMV5
EYFP-CD81 + Wnt7b-HA
I
Anti-Wnt7b Ab: R&D (AF3460)
DAPI
HA
Wnt7b
Merged
pCMV5
Wnt7b-HA

Figure S7

Figure S7. Related to Fig. 4 and 5. (**A)** The total number of particles in the exosome pellet (100,000 x g) were measured using NTA. (**B)** The total amount of protein in the exosome pellet was measured by Bradford assay. (**C)** Exosome characterization from porcupine-deficient L cells. Representative immunoblot of the cell lysate (Lys) and 100,000 x g pellet (Exo) analyzed for exosome markers and calnexin (CNX) (**D)** Quantification of **(C)**. Exosomes were collected from an equal number of cells, and equal volumes of exosome pellets (right two lanes) were used for comparison. Protein bands were quantified using ImageJ. **(E)** Representative TEM images of exosome pellet. Arrowheads indicate round vesicles. Scale bar, 200 nm. **(F)** Expression of Wnts in cortical neurons. RNA was isolated from cortical neurons at 0, 12, 24 and 33 h of culturing. A representative plot indicating mRNA expression relative to Wnt5a, determined by qPCR from 2 independent experiments is shown. **(G)** Efficiency of siRNA-mediated knockdown of Wnts. RNA was isolated from GFP-positive neurons after FACS. Relative mRNA expression was determined by qPCR. **(H)** Overlap of the localization of exosomes and Wnt7b. Cortical neurons electroporated with 2 μg of either pCMV5 or C-terminal HA-tagged Wnt7b (Wnt7b-HA) were treated with 10X CM containing CD81-EYFP, 24 h after plating for 30 minutes. Representative images of neurons stained with GFP (green), HA (yellow) and Tuj1 (red) antibodies from 20 neurons from 2 independent experiments are shown. Arrowheads indicate the localization of Wnt7b and exosomes. Scale bar, 20 μm **(I)** Wnt7b antibody characterization. MDA-MB-231 cells were transfected with 2 μg of either pCMV5 control or C-terminal HA-tagged Wnt7b (Wnt7b-HA). Cells were fixed after 48 h and immunostained with HA (green) and Wnt7b (yellow) antibodies. Scale bar, 20 μm.

Values are plotted as the mean ± SEM from 3 independent experiments **(A, B, D, G)**. Statistical significance: *$p<0.05$, **$p<0.01$, using unpaired t-test **(A, B)** or two-way ANOVA with Tukey's post-test **(D, G)**.

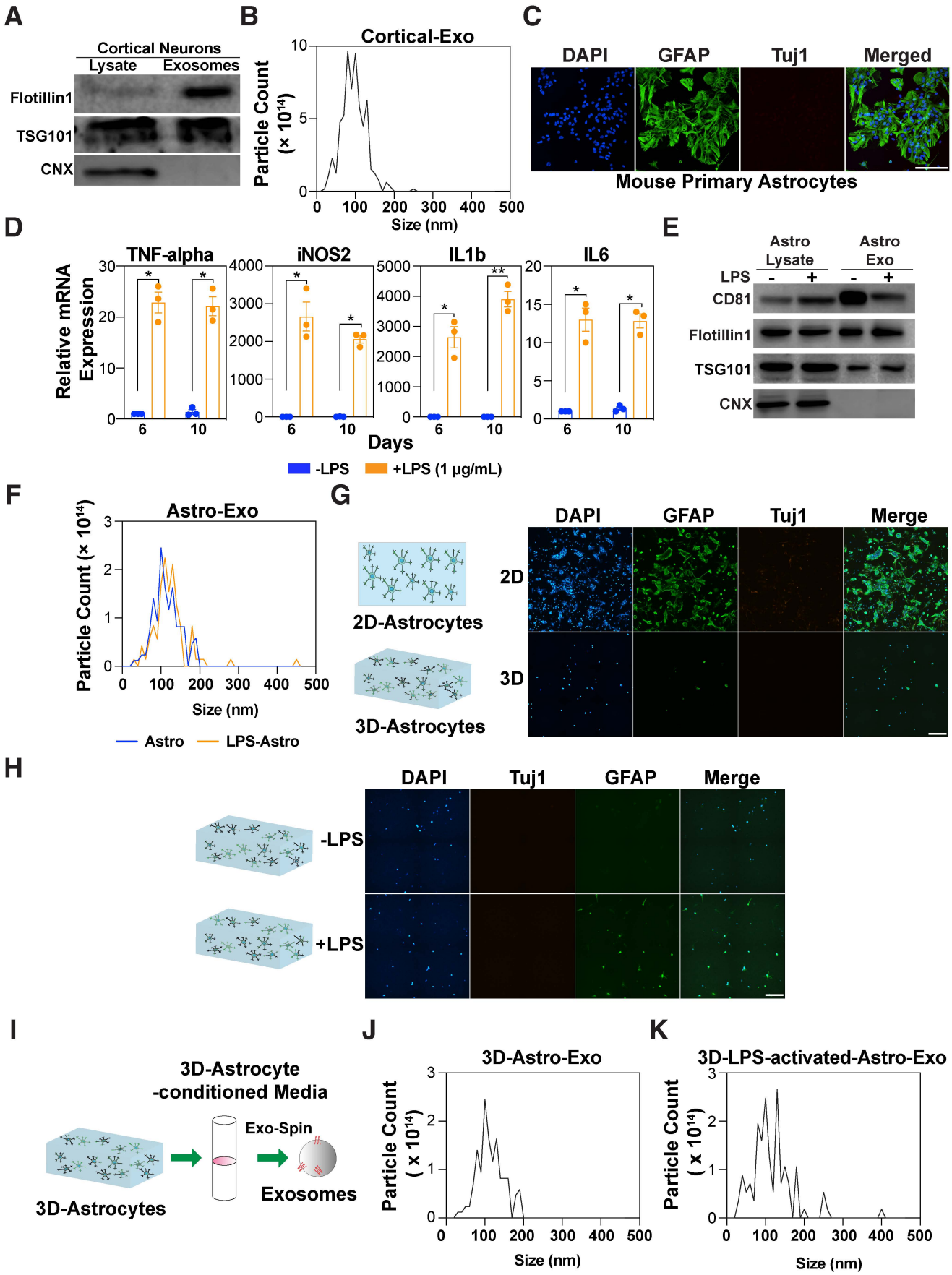
A
Cortical Neurons
Lysate
Exosomes
Flotillin1
TSG101
CNX
B
Cortical-Exo
Particle Count (× 10^14)
Size (nm)
C
DAPI
GFAP
Tuj1
Merged
Mouse Primary Astrocytes
D
TNF-alpha
iNOS2
IL1b
IL6
Relative mRNA Expression
Days
-LPS
+LPS (1 μg/mL)
E
Astro Lysate
Astro Exo
LPS
CD81
Flotillin1
TSG101
CNX
F
Astro-Exo
Particle Count (× 10^14)
Size (nm)
Astro
LPS-Astro
G
2D-Astrocytes
3D-Astrocytes
DAPI
GFAP
Tuj1
Merge
2D
3D
H
DAPI
Tuj1
GFAP
Merge
-LPS
+LPS
I
3D-Astrocyte
-conditioned Media
Exo-Spin
3D-Astrocytes
Exosomes
J
3D-Astro-Exo
Particle Count (x 10^14)
Size (nm)
K
3D-LPS-activated-Astro-Exo
Particle Count (x 10^14)
Size (nm)

Figure S8

Figure S8. Related to Fig. 6. (A) Immunoblot of exosomes and lysates from cortical neurons. **(B)** NTA of the exosome pellet. **(C)** Purity of primary astrocytes cultures. Enriched cultures of astrocytes from P1-P4 mouse pups were immunostained for the astrocyte marker, GFAP, and the neuronal marker Tuj1. Scale bar, 200 µm. **(D)** LPS activates mouse primary astrocytes. Astrocytes were treated with LPS (1 µg/mL), and RNA was isolated after 6 or 10 days. Relative expression of pro-inflammatory genes was measured by qPCR. **(E)** Immunoblot of lysates and the exosome pellet from primary astrocytes. **(F)** NTA of the exosome pellet. **(G)** Astrocytes are activated upon culturing in 2D plates. Representative immunofluorescence images of astrocytes grown either on a glass surface or in a soft collagen gel. Scale bar, 200 µm. **(H)** LPS activates astrocytes grown in 3D-collagen gels. Astrocytes were treated with LPS (1 µg/mL), fixed after 48 h and subsequently immunostained with GFAP and Tuj1 antibodies. Representative images are shown. Scale bar, 200 µm. **(I)** A schematic representation of exosome purification from astrocytes grown in a soft 3D-collagen gel. CM was collected after 6 days and subsequently exosomes were purified using Exo-spin^{TM} columns. **(J and K)** NTA of the exosomes.

NTA plots are from 1 representative experiment out of 3 independent purifications **(B, F, J, K)**. Values are plotted as the mean ± SEM from 3 independent experiments **(D)**. Statistical significance: *$p<0.05$, **$p<0.01$, using two-way ANOVA with Tukey's post-test (D).

Table S1: Genotyping primers and siRNAs

Genotyping Primers	
Gene	**Primers**
Pk1-F	CAGACTCCTGTCAACGCGATG
Pk1-R	CGCCTGCACAACAGCACTGTC
Pk1-MT-R	CCCCACAACGGGTTCTTCTGTTAG
Pk2-F	TGTGGCCACATTTGTTTTAGAGG
Pk2-R	CACACACTAACCAGAAATATCATC
Pk2-MT-R	CCCCACAACGGGTTCTTCTGTTAG
Vangl2	TGGCTGTCTTCTGCACTCAC
Vangl2-R	GCACCTTCTTGGTGCTCACT
Smurf1-F	CAGATGCTGAGGCAGGAGAATCATGAG
Smurf1-R	CAGTCCCCTCCCAACACACAATCAC
Smurf1-MT-R	AGTTCTAATTCCATCAGAAGCTGACTCTAG
Smurf2-F	TGCTATGGCTTCTGACTATTAAAAGGTC
Smurf2-R	CTTAAACATCAGCTCCTGAGTACACAAC
Smurf2-MT-R	AGTTCTAATTCCATCAGAAGCTGACTCTAG
Cre-F	TGACCGTACACCAAAATTTG
Cre-R	ATTGCCCCTGTTTCACTATC
List of siRNAs	
Gene	**Dharmacon Catalog #**
Dvl1	MQ-040910-00-0002
Dvl2	MQ-040921-01-0002
Dvl3	MQ-040922-01-0002
Frizzled1	MQ-063230-01-0002
Frizzled2	MQ-040443-01-0002
Frizzled3	MQ-048416-00-0002
Frizzled7	MQ-041631-01-0002
Frizzled8	MQ-045544-00-0002
Frizzled9	MQ-040416-01-0002
Prickle1	MQ-042729-01-0002
Prickle2	MQ-056882-02-0002
Vangl1	MQ-057276-01-0002
Vangl2	MQ-059396-01-0002
Wnt5a	MQ-065584-00-0002
Wnt5b	MQ-060428-01-0002
Wnt7a	MQ-058932-01-0002
Wnt7b	MQ-042139-00-0002
Porcupine	MQ-049203-01-0002
Wls	MQ-060922-01-0002

Table S2: List of antibodies

Reagent or Resource	Source	Identifier
Antibodies		
Mouse anti-MAP-2 (Clone AP20, 1:500)	Millipore	MAB3418
Mouse anti-Tubulin β 3 (Clone Tuj1, 1:3000)	Biolegend	801202
Mouse anti-Tau-1 (Clone PC1C6, 1:300)	Millipore	MAB3420
Mouse anti-TSG101 (1:500)	GeneTex	GTX70255
Mouse anti-Flotillin-1 (1:1000)	BD Transduction	618021
Mouse anti-CD81 (B-11, 1:1000)	Santa Cruz	sc-166029
Mouse anti-Prickle1 (F-5, 1:100)	Santa Cruz	Sc-393034
Mouse anti-Prickle2 (Clone 3B4.1, 1:100)	Millipore	MABN1529
Rabbit anti-GFAP (1:500)	Dako	Z0334
Rabbit anti-GFP (1:400)	Invitrogen	A11122
Rabbit anti-β III Tubulin (1:500)	Abcam	ab18207
Rabbit anti-Calnexin (1:2000)	(Jackson *et al*, 1994)	N/A
Rat anti-Vangl2 (Clone 2G4, 1:200)	Millipore	MABN750
Goat anti-Wnt7b (1:200)	R&D Systems	AF3460
Goat anti-GFP (1:1000)	Rockland	600-101-215
Donkey anti-goat DyLight™ 488 (1:1000)	Thermo Fisher Scientific	SA5-10086
Donkey anti-goat Alexa Fluor™ 647 (1:1000)	Thermo Fisher Scientific	A21447
Goat anti-Mouse Alexa Fluor® 488 (1:1000)	Invitrogen	A11029
Goat anti-Rabbit Alexa Fluor® 488 (1:1000)	Invitrogen	A11034
Goat anti-Mouse Alexa Fluor® 594 (1:1000)	Invitrogen	A11032
Goat anti-Rabbit Alexa Fluor® 594 (1:1000)	Invitrogen	A11012
Goat anti-rabbit Alexa Fluor™ 647 (1:1000)	Thermo Fisher Scientific	A21244
Donkey anti-Goat IgG-HRP (1:5000)	Jackson ImmunoResearch	705-035-147
Donkey anti-Mouse IgG-HRP (1:5000)	Jackson ImmunoResearch	715-035-152
Goat anti-Rat IgG-HRP (1:5000)	Jackson ImmunoResearch	112-035-175
IgG F2.A	(Pavlovic *et al.*, 2018)[1]	N/A
IgG	(Enderle *et al*, 2021)[2]	N/A

[1]Pavlovic Z, Adams JJ, Blazer LL, Gakhal AK, Jarvik N, Steinhart Z, Robitaille M, Mascall K, Pan J, Angers S *et al* (2018) A synthetic anti-Frizzled antibody engineered for broadened specificity exhibits enhanced anti-tumor properties. *MAbs* 10: 1157-1167

[2]Enderle L, Shalaby KH, Gorelik M, Weiss A, Blazer LL, Paduch M, Cardarelli L, Kossiakoff A, Adams JJ, Sidhu SS (2021) A T cell redirection platform for co-targeting dual antigens on solid tumors. *MAbs* 13: 1933690

Table S3: Primers for gene expression analysis

qPCR Primers		
Gene	**Forward Primer**	**Reverse Primer**
Wnt3a	CTCCTCTCGGATACCTCTTAGTG	GCATGATCTCCACGTAGTTCCTG
Wnt5a	CAACTGGCAGGACTTTCTCAA	CATCTCCGATGCCGGAACT
Wnt5b	CTGCTGACTGACGCCAACT	CCTGATACAACTGACACAGCTTT
Wnt7a	GGTGCGAGCATCATCTGTAA	CATTTGGGAGCCTTCTCCTATG
Wnt7b	GGATGCCCGTGAGATCAAA	GACACACCGTGACACTTACA
Prickle1	TCCCGAAACAAGGTCAGATTTA	TCTCTGGATCTGGCTGACT
Prickle2	CACTGCTTTGAGTCCCTGTATG	TCTGTAGCATGCCAGTGTTG
Vangl1	GCTGGCCTGAAAGTCTACAA	CGTGTTCGGCCTCTTCATAATA
Vangl2	ACTCGGGCTATTCCTACAAGT	TGATTTATCTCCACGACTCCCAT
Frizzled1	GCTGAGCTTGGAACTTTGTG	AGCCTCCAGCAACCAAA
Frizzled2	GCCGTCCTATCTCAGCTATAAGT	TCTCCTCTTGCGAGAAGAACATA
Frizzled3	ATGGCTGTGAGCTGGATTGTC	GGCACATCCTCAAGGTTATAGGT
Frizzled7	ATATCACGGCGAGAAAGGC	GCAGGATGGTCTGGTTGTAG
Frizzled8	ATGGAGTGGGGTTACCTGTTG	CACCGTGATCTCTTGGCAC
Frizzled9	TCCGCGTTGTGTTTCTTCT	GGCCAAGGAGTAGACATTGTAG
Dvl1	GAAGTCAGGCTTCAGCTGTT	CTACCTGTAAGTTCTGGAGGGA
Dvl2	CCATCCTTCCACCCTAATGTATC	CCATGTTCACTGCTGTCTCT
Dvl3	TGGTTTCATCCGCCATACC	ATCATGGTCGTGAAGCGATAG
Cd81	GTACCTGGAACTGGGAAACAA	CCCAGGAAGCCTACAAACAT
Smpd2	CAAAGGCTATCGCTCACCTATC	CTGGATTGGGTGTTTGGAGAA
Wntless	TGGGAAGCAGTCTAGCCTCC	GCAGCACAAGCCAAGGTGATA
Porcupine	GAGAAGGACCACCTGGAATG	ATAAGACATGGGCAGGTTCC
iNOS2	GGCAGCCTGTGAGACCTTTG	GCATTGGAAGTGAAGCGTTTC
IL1b	CAGGCAGGCAGTATCACTCA	TGTCCTCATCCTGGAAGGTC
IL6	ATGGATGCTACCAAACTGGAT	TGAAGGACTCTGGCTTTGTCT
TNF-α	ACGGCATGGATCTCAAAGAC	GTGGGTGAGGAGCACGTAGT
Gapdh	AGGTCGGTGTGAACGGATTTG	TGTAGACCATGTAGTTGAGGTCA